Materials & Design 260 (2025) 115148

Contents lists available at ScienceDirect

Materials & Design

journal homepage: www.elsevier.com/locate/matdes

58S mesoporous bioactive glass as a structural enhancer in α-TCP-based bone cements: gains in strength, challenges in bioactivity

Öznur Demir [a,b], Shahrbanoo Jahangir [c], Ezgi Irem Bektas [c], Mauro Alini [c], Aldo R. Boccaccini [d], Dagnija Loca [a,b,*]

[a] Institute of Biomaterials and Bioengineering, Faculty of Natural Sciences and Technology, Riga Technical University, Paula Valdena Street 3, k-1, Riga LV-1048, Latvia
[b] Baltic Biomaterials Centre of Excellence, Headquarters at Riga Technical University, Kipsalas Street 6A, Riga LV-1048, Latvia
[c] AO Research Institute Davos, 7270 Davos, Switzerland
[d] Institute of Biomaterials, Department of Materials Science and Engineering, University of Erlangen-Nuremberg, Cauerstrasse 6, 91058 Erlangen, Germany

ARTICLE INFO

Keywords:
Calcium phosphates
Calcium phosphate cement
Mesoporous bioactive glass
Bone tissue engineering
Osteogenic differentiation

ABSTRACT

Calcium phosphate bone cements (CPCs) are promising injectable bone substitutes but are limited by insufficient mechanical strength, prolonged setting time, and inadequate degradation profile. This study investigates the incorporation of mesoporous bioactive glass (58S MBG) into α-tricalcium phosphate (α-TCP)-based CPCs to enhance their physicochemical and biological performance. Composites containing 0–15 wt% MBG were fabricated and evaluated across multiple powder-to-liquid ratios. MBG addition extended final setting time from 9 to 42 min and increased compressive strength over threefold (from 3.39 to 10.40 MPa). Total porosity decreased (78 % to 61 %) while closed porosity increased, improving structural integrity. BG0 (0 %), BG5 (5 %), and BG9 (9 %) were selected for further *in vitro* testing with human mesenchymal stem cells. While BG0 supported early alkaline phosphatase (ALP) activity, BG5 and BG9 showed prolonged ALP response and upregulation of key osteogenic markers (ALP, COL1, RUNX2, SP7). Osteocalcin expression remained low across groups, indicating limited late-stage differentiation within the study period. The results demonstrate that MBG-modified CPCs offer enhanced mechanical performance and support osteogenic activity *in vitro*. These findings underscore the potential of MBG integration for optimizing CPC formulations aimed at minimally invasive bone regeneration applications.

1. Introduction

Surgeons frequently rely on donor bone or synthetic materials to address osseous defects resulting from conditions such as fractures, trauma, bone tumour resections, infections, or arthroplasty procedures [1]. While autografts and allografts are the conventional choices, they come with limitations, including donor site morbidity, limited availability, and potential immunogenicity [2]. To overcome these challenges, synthetic alternatives, including ceramics, polymers, and polymer-ceramic composites, have been developed and are widely used in clinical practice. These synthetic bone substitutes are available in diverse forms, including injectable pastes, mouldable cements, and pre-formed scaffolds, each tailored to specific clinical needs [3,4].

Among these options, calcium phosphate cements (CPCs) have emerged as a leading choice due to their biocompatibility, osteoconductivity, and ability to closely mimic the inorganic phase of natural bone [3,5]. The self-setting nature of CPCs, combined with their moldability and low-temperature processing, makes them ideal for minimally invasive applications. Despite these advantages, CPCs exhibit limitations in mechanical strength, setting time, and degradation rates, restricting their broader application in dynamic or load-bearing environments [6,7]. As highlighted in the authors' previous works [8] and supported by recent literature [6,7,9], the intrinsic structure and material properties of CPCs inherently constrain their mechanical performance, rendering them unsuitable for load-bearing applications. These limitations stem from their brittle nature, which compromises CPCs ability to withstand the dynamic stresses typically encountered in load-bearing environments.

To address these shortcomings, recent advancements have focused on enhancing the physicochemical and biological properties of CPCs by

* Corresponding author at: Institute of Biomaterials and Bioengineering, Faculty of Natural Sciences and Technology, Riga Technical University, Paula Valdena Street 3, k-1, Riga LV-1048, Latvia.
E-mail address: dagnija.loca@rtu.lv (D. Loca).

https://doi.org/10.1016/j.matdes.2025.115148
Received 3 July 2025; Received in revised form 23 October 2025; Accepted 13 November 2025
Available online 15 November 2025

incorporating various additives. Among these, bioactive glasses (BGs), particularly mesoporous bioactive glasses (MBGs), have emerged as promising candidates. MBGs not only improve the mechanical and rheological properties of CPCs but also enhance their biological performance by releasing bioactive ions such as silicon (Si), calcium (Ca), and phosphorus (P). These ions play a pivotal role in promoting bone regeneration by stimulating cellular signalling pathways that drive osteogenic differentiation, enhance extracellular matrix mineralization, and support osteoblast recruitment [10–12]. The high surface area and mesoporosity of MBG further amplify these effects by facilitating efficient ion release and providing extensive interaction sites for cellular activity. Additionally, MBG's unique structural properties enhance its versatility, making it suitable for drug delivery systems that enable sustained release of therapeutic agents [11].

Building on these advantages, incorporating MBG into CPCs helps address critical limitations, particularly by modulating degradation behaviour to match the rate of new bone formation [13]. Additionally, the bioactive properties of MBG have been linked to improvements in compressive strength, injectability, and setting time in some formulations, while also facilitating enhanced cellular interaction through the bioactive ion release [14]. However, despite these advancements, limited research has systematically investigated how MBG concentration influences both the structural properties and the *in vitro* biological response of CPCs, particularly in relation to human mesenchymal stem cells (hMSCs) differentiation. While *in vivo* studies have consistently demonstrated the osteoinductive potential of MBG through enhanced bone formation [8,15–22], its direct impact on osteogenic differentiation *in vitro* remains inconclusive. This variability in reported outcomes may stem from differences in MBG concentration, particle size, synthesis methods, and the weight or molar percentages of the bioactive glass, all of which affect the physicochemical properties, *in vitro* cellular responses and overall bioactivity of the composites [8,22,23].

Our previous work primarily focused on elucidating the effect of MBG particle size (<20, <38, and <100 μm) on the setting behaviour, microstructure, and mechanical performance of α-tricalcium phosphate (α-TCP)-based CPCs [14]. In contrast, the present study investigates the effect of MBG content (0–15 wt%) while maintaining a constant particle size (58S MBG < 20 μm). This approach decouples the compositional influence from particle-size-related effects, enabling a systematic evaluation of how increasing MBG content modulates the physicochemical and *in vitro* biological performance of α-TCP-based CPCs.

Given these knowledge gaps, this study systematically evaluates the effect of varying 58S MBG content (0, 2, 5, 7, 9, 10, 12, and 15 wt%) on the physicochemical properties and *in vitro* biological response of α-TCP-based CPC formulations, utilizing MBG particles with a fixed size of < 20 μm. By correlating key material characteristics, including setting time, mechanical properties, and phase composition, with the biological response of hMSCs, this study aims to determine whether the osteogenic differentiation observed *in vitro* aligns with MBG's well-established osteoinductive effects reported *in vivo*. Through this comprehensive assessment, the findings aim to contribute to the optimization of MBG-CPC composites for their application as injectable bone substitutes in bone tissue engineering.

2. Materials and methods

2.1. Preparation of α-tricalcium phosphate (α-TCP)

The α-TCP powder, renowned for its purity levels ranging from 98 % to 99 %, was synthesized following the methodology detailed in our previous research [24]. In summary, the process involved the synthesis of amorphous calcium phosphate (ACP) through a wet precipitation route. This entailed dissolving 21.39 g of ammonium hydrogen phosphate ($(NH_4)_2HPO_4$, Merck, Germany) and 57.38 g of calcium nitrate tetrahydrate ($Ca(NO_3)2{\cdot}4H_2O$) in 540 ml of distilled water, with subsequent adjustment of the solution's pH to approximately 10.0 at room temperature (RT) using a 7 M NaOH solution (Sigma Aldrich, USA). The two solutions were then mixed, followed by filtration and washing of precipitates. Subsequently, the obtained precipitate underwent lyophilisation (BETA 2–8 LCSplus, Martin Christ Freeze Dryers, Osterode, Germany) for 72 h. The ACP powder was then thermally treated at 650 °C for 1 h, with a heating and cooling rate of 10 °C/min, to obtain α-TCP powder. The obtained powder was then analysed by using X-ray diffractometer with a Cu Kα radiation source (λ = 1.5406 Å) at an operating voltage of 40 kV and a tube current of 15 mA (XRD, Miniflex 600 HR, Rigaku, Japan). Data were collected in the 2θ range of 3.016° to 59.999° with a step size of 0.0435°. The scanning mode was continuous, with a time per step of 2.98 s. The phase purity of the synthesized α-TCP powder was confirmed by matching the diffraction maxima to the ICDD file of α-TCP (no. 00-009-348) and by Rietveld refinement using Profex software (version 5.1, Solothurn, Switzerland). The specific surface area (SSA) of the synthesized powders was evaluated through nitrogen adsorption using a Quadrasorb SI (Quantachrome Instruments, USA) and determined via the Brunauer-Emmett-Teller (BET) method. Before analysis, the powders were degassed under vacuum conditions at room temperature for 24 h using an Autosorb Degasser (Quantachrome Instruments, USA).

2.2. Preparation of mesoporous bioactive glass (MBG)

The 58S mesoporous bioactive glass formulation, comprising 58 wt% SiO_2, 33 wt% CaO, and 9 wt% P_2O_5, was prepared. The synthesis of 58S MBG involves a meticulous process: initially, 4.0 g of P123 (Pluronic acid, a polyethylene glycol-polypropylene glycol-polyethylene glycol block copolymer, Sigma Aldrich, USA) was dissolved in 60.0 g ethanol along with 1.0 g 0.5 M HCl. Upon complete dissolution, 6.7 g of tetraethyl orthosilicate (TEOS) was added and allowed to mix for 30 min at RT. Subsequently, 4.637 g of $Ca(NO_3)_2{\cdot}4H_2O$ and 0.769 g of triethyl phosphate (TEP) were sequentially added at 30-minute intervals at RT. The resulting mixture (sol) was stirred at RT for 24 h. The sol was then transferred into a Petri dish and subjected to an evaporation-induced self-assembly process for one week. The dried gel was thermally treated at 700 °C for 5 h with a heating rate of 2 °C/min to yield the final 58S MBG product. The resultant 58S MBG was ground using a planetary ball mill at 30-minute intervals until the desired particle size was achieved. Subsequently, the ground powders were sieved to obtain fine (<20 μm) 58S MBG particles. XRD analysis was conducted to confirm the phase composition of 58S MBG. The measurements were performed using a Cu Kα radiation source (λ = 1.5406 Å) at an operating voltage of 40 kV and a tube current of 15 mA. The diffraction data were collected over a 2θ range of 3.016° to 59.999° with a step size of 0.0435° and a time per step of 2.98 s in continuous scan mode. Scanning transmission electron microscopy (STEM, Thermo Fisher PV3-137, USA) was used to examine the morphology of the obtained 58S MBG powders. The samples were dispersed in ethanol, drop-cast onto a carbon-coated copper grid, and dried at room temperature before imaging. STEM micrographs were acquired at an accelerating voltage of 30 kV and 0.1nA current. The SSA, pore size, and pore volume distribution of the synthesized MBG powders were assessed following the methodology outlined in the previous section.

2.3. Preparation and characterization of the α-TCP/MBG composites

The general experimental workflow, including preparation and characterization steps, is illustrated in Fig. 1. The α-TCP/MBG composite cements were prepared by combining a solid and a liquid phase. The solid phase was prepared by mixing the obtained α-TCP powder and 58S MBG powder, up to a maximum of 15 wt% of 58S MBG content. The liquid phase consisted of a mixture of 1 M $Na_2HPO_4{\cdot}2H_2O$ (Sigma Aldrich, USA, Mw: 177.99 g/mol) and 1 M $NaH_2PO_4{\cdot}2H_2O$ (Sigma Aldrich, USA, Mw: 156.01 g/mol) solution, with a pH value of 7.0 as described in our previous work [24]. The powder phase was then mixed

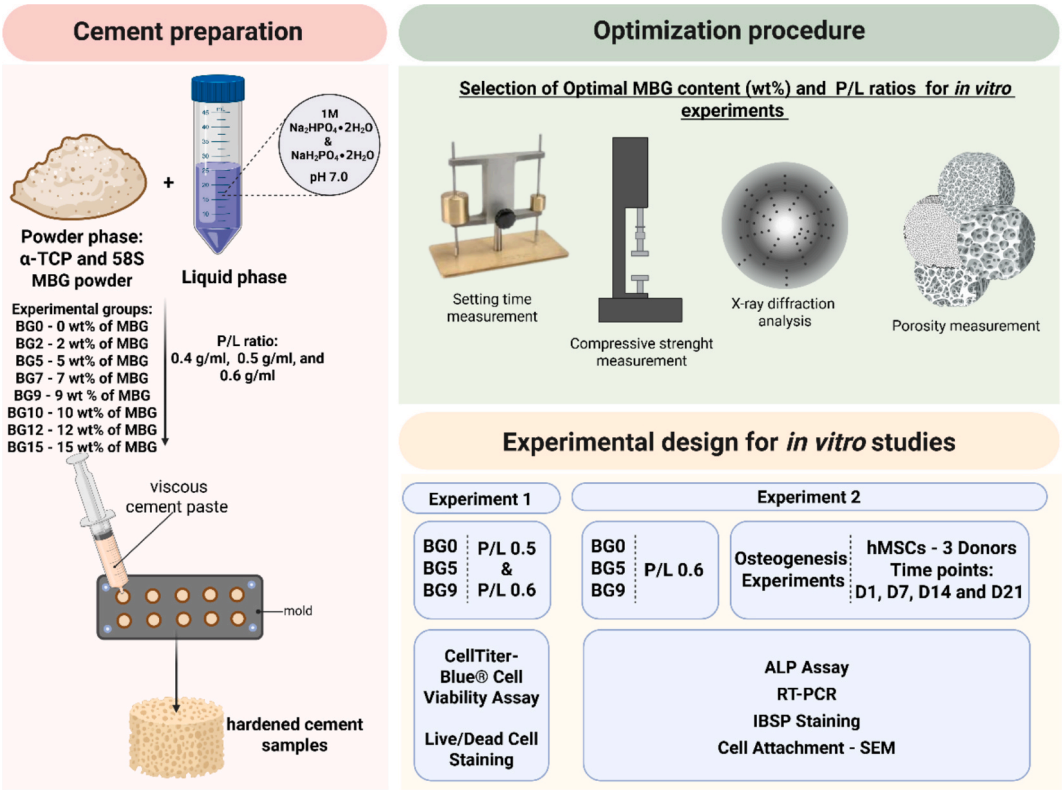

Fig. 1. Experimental design: Cement preparation, optimization procedure, and experimental design for *in vitro* studies (created by using Biorender).

with the liquid phases for 45 s at three different powder/liquid (P/L) ratios (0.4 g/ml, 0.5 g/ml and 0.6 g/ml) to obtain homogenous cement pastes. α-TCP powder cements (58S MBG powder free cements) labelled as BG0 were also prepared as a comparison following the same procedure for α-TCP/MBG cements. The prepared composite cement samples contain 100, 98, 95, 93, 91, 90, 88, or 85 wt% of α-TCP powder and 0, 2, 5, 7, 9, 10, 12, 15 wt% of 58S MBG powder, respectively (Table 1). Their respective abbreviations are BG0, BG2, BG5, BG7, BG9, BG10, BG12, and BG15.

To determine the setting time, freshly synthesized powders were thoroughly mixed with the liquid phase for 45 s before being cast into stainless steel moulds with dimensions of 5 mm in height and 10 mm in diameter. The samples were allowed to rest for 2 min before the setting time measurement was conducted using a Gillmore needle method (initial setting time measuring needle: mass = 113.4 ± 0.5 g, diameter = 2.12 ± 0.05; final setting time measuring needle: mass = 453.6 ± 0.5 g, diameter = 1.06 ± 0.05) in accordance with the ASTM C266-89 standard. Briefly, the needle was gently dropped onto the flat surface of the sample. The test continued until the sample no longer exhibited a complete circular indentation greater than 1 mm under either needle.

The phase formation of the cement formulations after setting was analysed using XRD employing the following parameters: 40 kV and 15 mA, with a step size of 0.0435°, ranging from 3° to 60° 2θ degrees, and a time per step of 2.98 s.

The compression test using a computer-controlled Universal Testing Machine (H1K–S by Tinius Olsen, USA) was conducted on cylindrical samples (20 mm in height and 10 mm in diameter). The specimens were kept in their moulds at 37 °C for 24 h, after which compressive strength was measured in the dry state. The load–displacement curve was recorded using a constant crosshead speed of 1 mm/min. The test continued until the samples reached 15 % deformation. The ultimate compressive strength (MPa) was determined as the maximum stress before failure.

The porosity of the samples was determined utilizing Archimedes' method, which hinges on the principle that the buoyant force exerted on a fully immersed object is equivalent to the weight of the fluid displaced [25]. The following equations were employed to compute the percentages of open (P_O), closed (P_C), and total (P_T) porosity:

$$P_O = (m_1\text{-}m_0)/(m_1\text{-}m_2)* 100$$

$$\rho Ap = m_0/(m_1\text{-}m_2)$$

$$P_T = 100\text{-}((\rho Ap*100)/\rho Th))$$

$$P_C = P_T - P_O$$

where m_1 — weight of impregnated sample, m_0 — weight of the dry sample, m_2 — weight of impregnated sample in the water, ρAp — the apparent density of the sample, ρTh — the theoretical density of the sample (measured by using the pycnometer ULTRAPYC™ 1200e (Quantachrome Instruments, USA)). Three replicate samples were analysed to determine both the porosity and densities (apparent and theoretical) of the prepared compositions.

Table 1
Composition of the cement formulations, including the weight percentages of 58S MBG and α-TCP powders, the liquid phase composition, and the powder-to-liquid (P/L) ratio used throughout the experiments. The abbreviations correspond to different formulations based on the MBG content (wt. %).

Abbreviation	MBG (wt. %)	A-TCP (wt. %)	Liquid Phase	P/L ratio (g/mL)
BG0	–	100	1 M $Na_2HPO_4{\cdot}2H_2O$ and 1 M $NaH_2PO_4{\cdot}2H_2O$ mixture at pH 7.0	0.4, 0.5 and 0.6
BG2	2	98		
BG5	5	95		
BG7	7	93		
BG9	9	91		
BG10	10	90		
BG12	12	88		
BG15	15	85		

2.4. In vitro bioactivity test

Disc-shaped cement samples (10 mm in diameter and 2 mm in thickness) were soaked in simulated body fluid (SBF) at 37 °C to evaluate phase transformation and biomineralisation. SBF, which closely mimics the ionic composition of human blood plasma, was prepared following the method developed by Kokubo et al. [26]. The samples were incubated at a ratio of 0.1 g of material per mL of SBF for 7 and 14 days. After incubation, the samples were gently rinsed with deionized water and dried at room temperature prior to characterization. The formation of the calcium-deficient hydroxyapatite (CDHAp) layer on the sample surfaces was examined using scanning electron microscopy (SEM, ThermoFisher PV3-137, USA) at an acceleration voltage of 30 kV. Prior to SEM observation, the samples were sputter-coated with carbon (C) to enhance conductivity. Phase transformation during the incubation period was analysed using X-ray diffraction (XRD, PANalytical Aeris diffractometer, Netherlands). The following ICDD reference files were used for phase identification: no. 00–026-1056 for octacalcium phosphate (OCP) and no. 00–009-0432 for calcium-deficient hydroxyapatite (CDHAp). Additional phases present in the samples were also examined. Phase composition changes over the incubation period were analysed and quantified using Profex software (version 5.1, Solothurn, Switzerland) [27].

2.5. In vitro cellular assessment

2.5.1. Isolation and expansion of human mesenchymal stem cells from bone marrow (hMSCs)

Primary human mesenchymal stem cells (hMSCs) were isolated from bone marrow aspirates obtained from three male donors aged between 42 and 66 years. All donors provided written informed consent. According to the Swiss Human Research Act, research using anonymized biological material and/or anonymized health-related data does not require ethics committee approval. Therefore, ethical approval was not required for this study. General consent obtained from the patients also included permission for the anonymization and use of biological material and health-related data (See Institutional Review Board Statement and Informed Consent Statement for details). Isolated cells were seeded at 50,000 cells/cm^2 into 300 cm^2 tissue culture flasks in Minimum Essential Medium Eagle, Alpha Modification (α-MEM; Gibco, Thermo Fisher, Zürich, Switzerland) containing 10 % fetal bovine serum (FBS, Gibco, Thermo Fisher, Zürich, Switzerland), 1 % penicillin- streptomycin (Pen-Strep, Gibco), and 0.1 % recombinant human basic Fibroblast Growth Factor (FGF2, Fitzgerald Industries International, Acton, MA, USA). Cells were maintained at 37 °C in 5 % CO_2 and 95 % humidity. Throughout the study, cells from three different donors were used. Experiments were conducted using cells at passage numbers ranging from 1 to a maximum of 3.

2.5.2. Cell proliferation measurement

Samples for the cell proliferation tests were prepared using two different P/L ratios (P/L 0.5 and P/L 0.6) with three different composite compositions (BG0, BG5 and BG9). Before testing, the samples were sterilized by incubation in 70 % ethanol for 30 min, followed by ultraviolet (UV) exposure for 1 h (30 min on each side). Prior to cell seeding, the cement composites were incubated in α-MEM supplemented with 10 % FBS and 1 % -Pen-Strep for 3 h. In addition, another set of cement composites was pre-incubated in pure FBS for 3 h before cell seeding to evaluate potential differences in initial cell attachment. Cells were seeded at a density of $2x10^5$ cells/cement sample. Cell proliferation was assessed using CellTiter-Blue® assay (Promega, Promega Corporation, Madison, WI, USA) according to the manufacturer's instructions. Cell proliferation was quantified as mean fluorescence intensity (560_{Ex}/590_{Em}) on days 1 and 3. All experiments were repeated in triplicate and each group had 3 replicates.

2.5.3. Live/Dead assay

The viability of cells seeded on cement composites was assessed using Live/Dead staining. After 1 day, 3 days and 7 days of incubation, cells were stained with 2 mM Calcein AM (λex = 488 nm) (Invitrogen, Thermo Fisher) and 4 mM ethidium homodomer-1 (λex = 561 nm) (EthD-1-, Invitrogen, Thermo Fisher) in PBS for 30 min. The stained cells were then immediately analysed using confocal microscopy (LSM800, Zeiss AG, Feldbach, Switzerland).

2.5.4. Osteogenic differentiation studies

In vitro osteogenic differentiation was conducted on cement composites (P/L 0.6 for BG0, BG5, and BG9). hMSCs were seeded on top of the cement at a density of $2x10^5$ cells per cement sample in a complete growth medium and incubated overnight (n = 3 donors, with 2 replicates per donor). Next day, the medium was changed to differentiation medium, containing DMEM (Gibco) supplemented with 10 % v/v FBS (Corning), 1 % v/v Pen-Strep (100 U/mL of penicillin, 100 μg/mL of streptomycin, Gibco), 50 μg/mL l-Ascorbic acid 2-phosphate sesquimagnesium salt hydrate (AA2P, Sigma), 5 mM beta-glycerol phosphate (BGP, Sigma), and 10 nM Dexamethasone (Dexa, Sigma). The differentiation medium was changed twice per week.

2.5.4.1. Alkaline phosphatase (ALP) activity and DNA content. Cells were lysed using 0.1 % v/v Triton X-100 (Sigma-Aldrich) in 10 mM TrisHCl in order to quantify the ALP activity and DNA content at days 1, 7, 14 and 21. ALP activity was assessed by adding alkaline buffer solution, a substrate solution (25 mg/mL phosphate substrate in 1 mM diethanolamine buffer containing 0.5 mM $MgCl_2$, pH 9.8, Sigma-Aldrich) and deionised water to the cell lysate. The enzymatic reaction was carried out at 37 °C for 15 min and then stopped by the addition of 0.1 M NaOH solution. The absorbance was measured at 405 nm using a microplate reader (Infinite® 200 PRO microplate reader, TECAN). DNA content was determined using DNA quantification assay (CyQUANT™ Assay, ThermoFisher) following the manufacturer's protocol. Fluorescence was measured at 480 nm excitation wavelength and 520 nm emission wavelength using the same microplate reader (Infinite® 200 PRO microplate reader, TECAN). A DNA standard curve was generated for quantification. ALP activity was normalized to the DNA content to ensure accurate activity measurements.

2.5.4.2. RNA isolation and reverse transcription-quantitative polymerase chain reaction (RT-qPCR). Osteogenic-related gene expression levels were evaluated via RT-qPCR on days 1, 7, 14, and 21 during the incubation of the cement composites in osteogenic medium. Total RNA was extracted from cement composites (P/L 0.6 for BG0, BG5, and BG9) using TriReagent® (Molecular Research Center Inc.), following the manufacturer's protocol. RNA concentration and purity were determined using a NanoDrop UV–Vis spectrophotometer (Thermo Fisher, USA). Subsequently, 0.25 μg of RNA was reverse-transcribed into cDNA using the Vilo Superscript kit (Invitrogen, USA) and a Thermocycler (Mastercycler gradient, Eppendorf, USA) according to the provided guidelines. For the qPCR analysis, a 10 μl reaction mixture was prepared, consisting of 5 μl TaqMan Gene Expression Master Mix (Thermo Fisher, USA), forward and reverse primers (45 μM each), TaqMan probe (12.5 μM), diethylpyrocarbonate (DEPC) water, and 5 ng of cDNA. The reactions were carried out in 384-well plates under a standard PCR program: an initial incubation at 50 °C for 2 min, polymerase activation at 95 °C for 10 min, followed by 40 cycles of denaturation at 95 °C for 15 s and annealing at 60 °C for 1 min. Relative gene expression levels were determined using the $2^{-\Delta\Delta Cq}$ method, with RPLP0 serving as the reference gene. Gene expression levels were normalized to day 1 samples from the same experimental condition and donor. The evaluated genes included RUNX2, ALPL, SP7, COL1A1, and OC. The TaqMan Gene Expression Assay IDs (Thermo Fisher, USA) and the sequences for the primers and probes used are provided in Table 2.

Table 2
Primer and probe (forward, reverse and probe sequence) and TaqMan Gene Expression Assays (Applied Biosystem Assay ID) for gene expression analysis.

	Gene	Forward primer sequence	Reverse primer sequence	Probe sequence	Assay ID
Primer and probe	RPLP0	5′-TGG GCA AGA ACA CCA TGA TG-3′	5′-CGG ATA TGA GGC AGC AGT TTC-3′	5′-AGG GCA CCT GGA AAA CAA CCC AGC-3′	–
	RUNX2	5′-AGC AAG GTT CAA CGA TCT GAG AT-3′	5′-TTT GTG AAG ACG GTT ATG GTC AA-3′	5′-TGA AAC TCT TGC CTC GTC CAC TCC G-3′	–
	COL1A1	5′–CCC TGG AAA GAA TGG AGA TGA T-3′	5′-ACT GAA ACC TCT GTG TCC CTT CA-3′	5′-CGG GCA ATC CTC GAG CAC CCT – 3′	–
	OC (BGLAP)	5′-AAG AGA CCC AGG CGC TAC CT-3′	5′-AAC TCG TCA CAG TCC GGA TTG-3′	5′-ATG GCT GGG AGC CCC AGT CCC-3′	
TaqMan Gene Expression Assays	ALPL	–	–	–	Hs00758162_m1
	SP7	–	–	–	Hs00541729_m1

2.5.4.3. Integrin-binding sialoprotein (IBSP) staining. Cement samples (P/L 0.6 BG0 and BG9) designated for integrin-binding sialoprotein (IBSP, Thermo Fisher, #PA5-114915, USA) immunofluorescence staining were collected on days 1 and 21. Fixation was performed by incubating the samples in 4 % formalin solution for 30 min under a sterile hood. Following fixation, the samples were washed three times with phosphate-buffered saline (PBS) to remove residual formalin. After the final wash, 70 % ethanol was added to the samples, which were subsequently stored at 4 °C for the further processing. Fixed samples were permeabilised using PBS-T (0.1 % Triton X-100 in 1 × PBS) by incubating them in the solution for 15 min at room temperature. The permeabilised samples were then washed three times with PBS. To block nonspecific binding sites, 2 % v/v bovine serum albumin (BSA) in PBS was added to the samples, followed by incubation for 60 min at room temperature. A primary antibody targeting IBSP was prepared by diluting it 1:250 in 0.1 % BSA in PBS-T. The prepared antibody solution (250 μL) was applied to the cement samples, which were then incubated overnight at 4 °C. After overnight incubation, the cement samples were washed three times with PBS to remove the unbound primary antibody. A fluorescence dye-labelled secondary antibody (diluted 1:1000 in 0.1 % BSA in PBS-T) was added (250 μL) and incubated for 45 min at room temperature, protected from light to prevent photobleaching. Afterward, the samples were washed three times with PBS. Counterstaining was performed using 4′,6-diamidino-2-phenylindole (DAPI) diluted 1:500 in PBS. The samples were incubated with DAPI for 30 min, washed with PBS, and subsequently imaged using confocal microscopy (LSM800, Zeiss AG, Feldbach, Switzerland).

2.6. Statistical analysis

Results are presented as mean values from at least 3 replicate samples ± standard deviation, unless otherwise specified. Differences between the groups were analysed using one-way ANOVA for single time points or two-way ANOVA for comparisons across multiple time points. Experiments were conducted at least three times, using bone cement composites seeded with hMSCs derived from different donors for each replicate. Statistical analyses were performed using GraphPad Prism 8 (GraphPad Software Inc., USA). Statistical significance is indicated as follows: *$p < 0.05$, **$p < 0.01$, ***$p < 0.001$, ****$p < 0.0001$, and ns = not significant. To explore potential relationships between material structure and biological response, correlation coefficients (r) were computed using group mean values (BG0, BG5, BG9) for each pair of physicochemical and biological parameters. Pearson's r was used to quantify the direction and relative strength of these linear relationships ($r = -1$ to $+1$). Given the limited number of groups ($n = 3$), these results were interpreted descriptively as indicators of trend direction rather than inferential statistics.

3. Results and discussions

3.1. Characterization of synthesized α-TCP and 58S MBG powders

The structural and morphological characteristics of the synthesized α-TCP and 58S MBG powders were thoroughly examined to evaluate their suitability for CPC formulation. The XRD patterns of the α-TCP powder (Fig. 2(A)) exhibit sharp and well-defined peaks, matching the reference patterns for α-TCP, confirming the successful synthesis of the desired phase. In contrast, the diffractogram of the 58S MBG shows a broad halo peak, characteristic of its amorphous nature. This distinction between the crystalline α-TCP and amorphous 58S MBG highlights their complementary roles within the CPC matrix, where α-TCP provides structural integrity and 58S MBG enhances bioactivity through ion release. SEM analysis of the α-TCP powder (Fig. 2(B)) reveals irregularly shaped particles with a rough surface texture, consistent with low-temperature synthesized α-TCP [24]. The 58S MBG powder, sieved through a 20 μm mesh, exhibits uniformly fine particles (Fig. 2(D)), confirming the particle size distribution suitable for homogeneous mixing within the CPC matrix. Additionally, STEM images of the 58S MBG powder (Fig. 2(E) and (F)) provide further insights into its mesoporous structure, which is expected to enhance ion release and interaction with cells [28]. BET analysis (table in Fig. 2(C)) shows that 58S MBG possesses a significantly higher surface area (125.72 ± 13.57 m^2/g) along with a large pore volume and fine average pore size (characteristic of its mesoporous structure), whereas α-TCP exhibits a much lower surface area (11.32 ± 0.39 m^2/g) compared to 58S MBG. This high surface area and mesoporosity of MBG are critical for facilitating bioactive ion release, contributing to enhanced cellular responses and osteogenic differentiation [29]. The α-TCP powder, with its moderate surface area, supports the setting reaction and structural stability of the CPC [30].

3.2. Characterization of prepared cement samples

3.2.1. Elevated bioactive glass concentrations inhibit the setting of the cement

The addition of 58S MBG powder contributed to the notable increment of the setting time in all tested groups of cements (Fig. 3(A)). Increased MBG concentrations led to a noticeable prolongation of both initial and final setting times across all tested powder-to-liquid (P/L) ratios (0.4, 0.5, and 0.6 g/mL). This effect is attributed to the slower reactivity of 58S MBG particles compared to the highly reactive α-TCP phase, which hinders the overall progression of the setting reaction [14]. Notably, cement composites with 12 wt% and 15 wt% 58S MBG at P/L ratios of 0.5 and 0.6 failed to harden, indicating that excessive MBG concentrations inhibit the crystallization of calcium-deficient hydroxyapatite (CDHAp), which is essential for the cement setting process. This observation aligns with previous findings that the presence of MBG introduces additional surface area and ion exchange sites, thereby slowing the cement setting kinetics [14,31]. For clinical applications, this

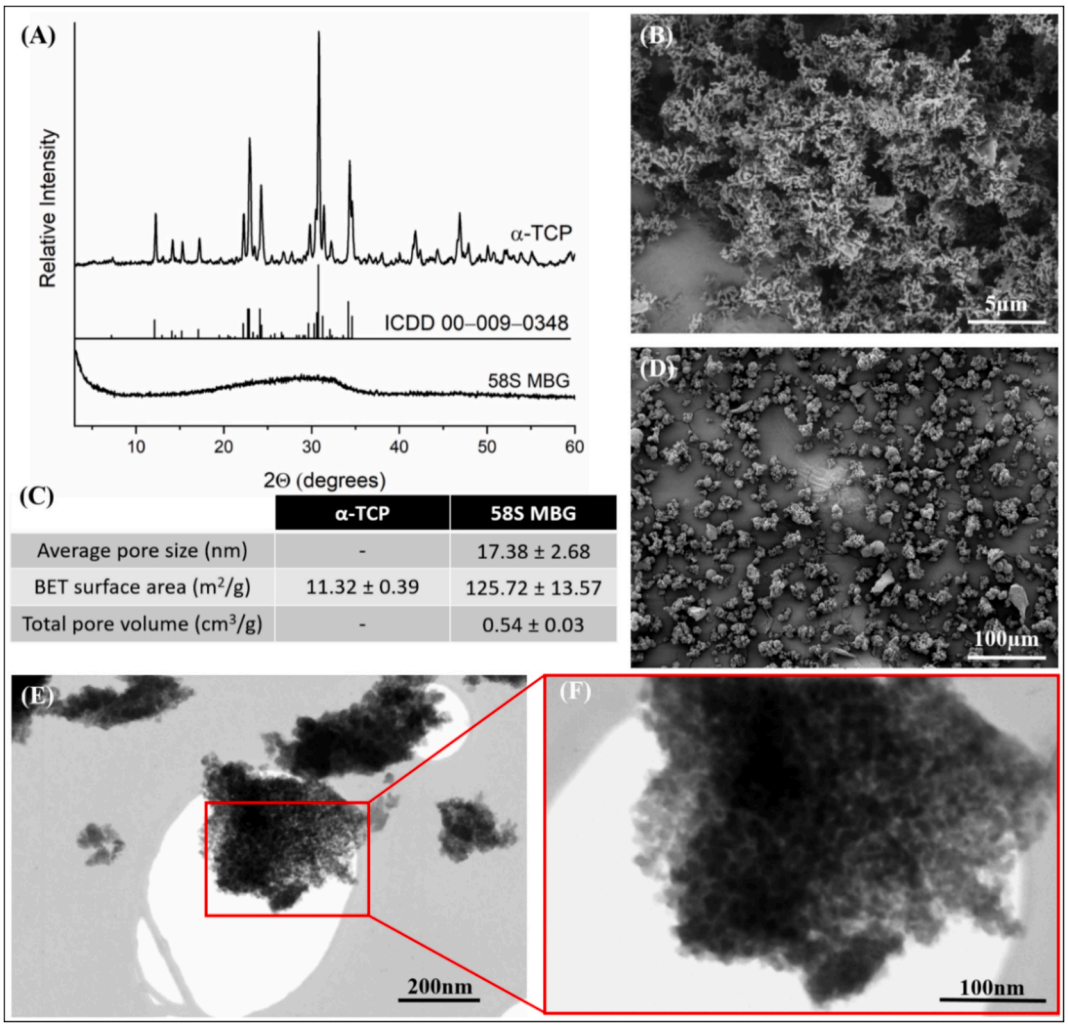

	α-TCP	58S MBG
Average pore size (nm)	-	17.38 ± 2.68
BET surface area (m^2/g)	11.32 ± 0.39	125.72 ± 13.57
Total pore volume (cm^3/g)	-	0.54 ± 0.03

Fig. 2. Characterization of the synthesized powders: (A) XRD patterns of α-TCP, with reference peaks for α-TCP, and 58S MBG; (B) Representative SEM micrograph of α-TCP powder; (C) Table summarizing the Brunauer-Emmett-Teller (BET) analysis of α-TCP and 58S MBG powders; (D) Representative SEM micrograph of 58S MBG powder, sieved using a 20 μm mesh-sized sieve; (E) and (F) Representative STEM micrographs of the synthesized 58S MBG powder.

prolonged setting time may be advantageous for certain procedures requiring extended working time [17], but higher concentrations (>10 wt%) may limit the feasibility of the material for time-sensitive applications.

The mechanical properties of the CPC composites were significantly influenced by 58S MBG weight percentage amount and the P/L ratio, as shown in Fig. 3 (B). Compressive strength measurements revealed a non-linear relationship between 58S MBG content and mechanical performance. Groups with lower 58S MBG amount (2–9 wt%) exhibited an increase in compressive strength particularly at the higher P/L ratios (0.5 and 0.6 g/mL). This improvement can be attributed to the homogeneous distribution of 58S MBG particles within the matrix, enhancing the structural integrity of the composite. However, further increasing 58S MBG content to ≥ 12 wt% resulted in a modest decline in compressive strength. This decrease is associated with the micro porosity induced by the high 58S MBG content, as observed in Fig. 5. At these higher concentrations, the excessive MBG fraction disrupts the cohesion of the cement matrix by diluting the reactive α-TCP phase and retaining additional liquid within the mesoporous network. This leads to incomplete α-TCP hydrolysis, weak interparticle bonding, and the formation of micropores and interfacial defects that act as stress concentrators. These structural irregularities explain the pronounced drop in compressive strength observed for BG15, despite its higher MBG loading. The higher variability in compressive strength observed for ≥10 wt% MBG likely arises from incomplete setting and heterogeneous matrix densification under dry conditions, rather than intrinsic material instability. In theory, lower porosity should enhance compressive strength [32]; however, beyond 9 wt% 58S MBG, the composites exhibit microstructural inhomogeneity and interfacial weaknesses that act as stress concentrators, disrupting the continuity of HAp crystal growth [33,34]. This typical trade-off in mesoporous glass-containing CPCs results in decreased mechanical integrity despite a trend toward reduced overall porosity. The mesoporous structure of 58S MBG, while beneficial for bioactivity, compromises mechanical stability when present in excessive amounts, particularly at higher P/L ratios. These results suggest that optimizing 58S MBG content is critical for achieving a balance between mechanical performance and biological functionality. For clinical applications, the compressive strength of BG5 and BG9 composites (approximately 3.39 MPa for P/L 0.5 and 4.99 MPa for P/L 0.6 and 9.42 MPa for P/L 0.5 and 10.40 MPa for P/L 0.6, respectively) falls within the range suitable for non-load-bearing applications, such as injectable bone fillers for minimally invasive procedures. However, groups with ≥ 12 wt% MBG failed to meet the minimum mechanical requirements, further justifying their exclusion from subsequent analyses.

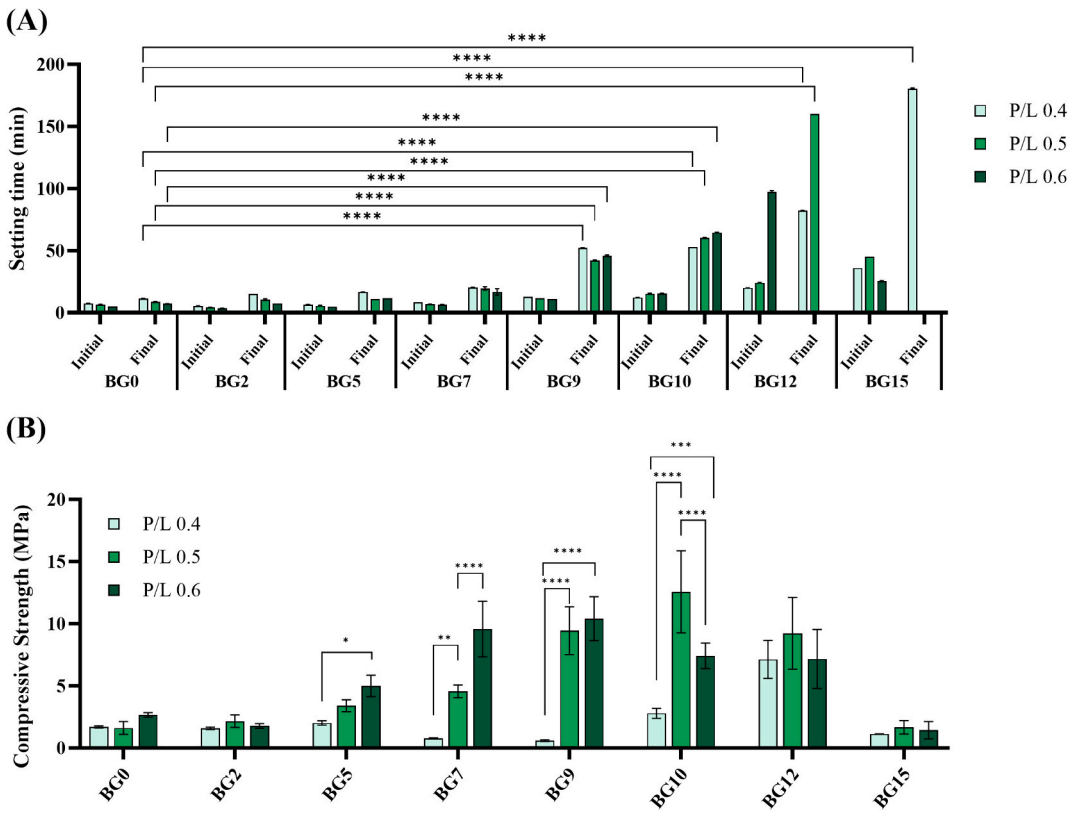

Fig. 3. (A) Initial and final setting time of the tested bone-cement composites (n = 3; mean ± SD). Statistical analysis was performed using one-way ANOVA followed by Tukey's multiple-comparison test. Although several pairwise differences were statistically significant, only comparisons between BG0 (control) and the corresponding MBG-added samples at each P/L ratio are indicated for clarity (*p < 0.05, **p < 0.01, ***p < 0.001, ****p < 0.0001). (B) Compressive strength of cement composites after setting (n = 5; mean ± SD). Asterisks denote statistically significant differences.

3.2.2. *High 58S MBG concentrations disrupt phase composition and crystallization*

XRD analysis of the cement composites after their setting revealed distinct phase compositions influenced by 58S MBG concentration and P/L ratios (Fig. 4). The presence of both octacalcium phosphate (OCP) and calcium-deficient hydroxyapatite (CDHAp) was confirmed across all groups, with their relative proportions significantly influenced by the MBG content. As shown in Table 3, BG0 (without MBG added bone cement) exhibited the highest OCP content, reaching 32.4 % and 33.0 % at P/L ratios of 0.4 and 0.6, respectively. Correspondingly, the formation of CDHAp in BG0 remained lower (67.6 %–67.0 %), indicating limited phase transformation of OCP to CDHAp in the absence of MBG. This indicates that in the absence of 58S MBG, the formation of CDHAp is limited, leaving OCP as the most abundant phase. This observation highlights the inability of the CPC matrix without 58S MBG to effectively transition from OCP to CDHAp during the setting process, which may limit its immediate structural stability and bioactivity. However, OCP is known to serve as a beneficial precursor phase for bone mineralization and regeneration due to its ability to gradually transform into CDHAp under physiological conditions [35–37]. This gradual transformation facilitates ion release, promotes osteoconductivity, and supports early bone regeneration [35,38].

In contrast, the incorporation of 58S MBG at moderate concentrations (e.g., BG5 and BG9) led to a favourable balance between OCP and CDHAp phases. These groups displayed reduced OCP diffraction maxima intensity compared to BG0, with peaks observed at 2Θ 4.7°, accompanied by an increase in CDHAp formation with peaks observed at 2Θ 32.2 ° and 2Θ 32.9 °, especially at P/L ratios of 0.5 and 0.6. This qualitative shift was further supported by the quantitative phase analysis presented in Table 3, where BG9 exhibited up to 94.92 ± 0.66 % CDHAp and only 5.09 ± 0.66 % OCP at P/L 0.6, while BG5 showed 93.63 ± 1.94 % CDHAp and 6.38 ± 1.94 % OCP at the same ratio. This shift suggests that 58S MBG contributes to a more efficient setting reaction by facilitating the crystallization of CDHAp while maintaining a sufficient amount of OCP for sustained ion release and bioactivity. This acceleration can be explained by the ionic and surface effects of MBG. During the setting process, MBG rapidly releases calcium, phosphate, and silicate ions, which increase local supersaturation and promote nucleation of apatite phases. Additionally, silanol groups on the MBG surface act as heterogeneous nucleation sites, further enhancing the transformation from OCP to CDHAp. Clinically, this combination is advantageous as it ensures immediate structural stability provided by CDHAp and long-term bioactivity supported by the conversion of OCP to CDHAp [39]. At higher 58S MBG concentrations (≥10 wt%), the XRD patterns showed suppressed formation of both OCP and CDHAp. This effect was more pronounced at lower P/L ratios, where the excessive porosity induced by high MBG content disrupted the crystallization process. The lack of significant OCP and CDHAp phases in these groups compromises both the bioactivity and mechanical integrity of the cement, making them unsuitable for further analysis.

3.2.3. *Porosity and phase transformation determine bioactivity and mechanical integrity*

As shown in Fig. 5, the addition of 58S MBG significantly influenced the porosity characteristics of the composites, including total porosity (P_T), open porosity (P_O), and closed porosity (P_C). The total porosity of the composites demonstrated a significant dependence on 58 MBG content and P/L ratio. At P/L 0.4, BG0 exhibited the highest total porosity (77.82 ± 0.86 %), which progressively decreased with the incorporation of 58S MBG. BG5 and BG9, with moderate 58S MBG addition, displayed reduced total porosity (71.50 ± 0.50 % and 69.88 ± 1.05 %, respectively), indicating improved structural packing. Similar

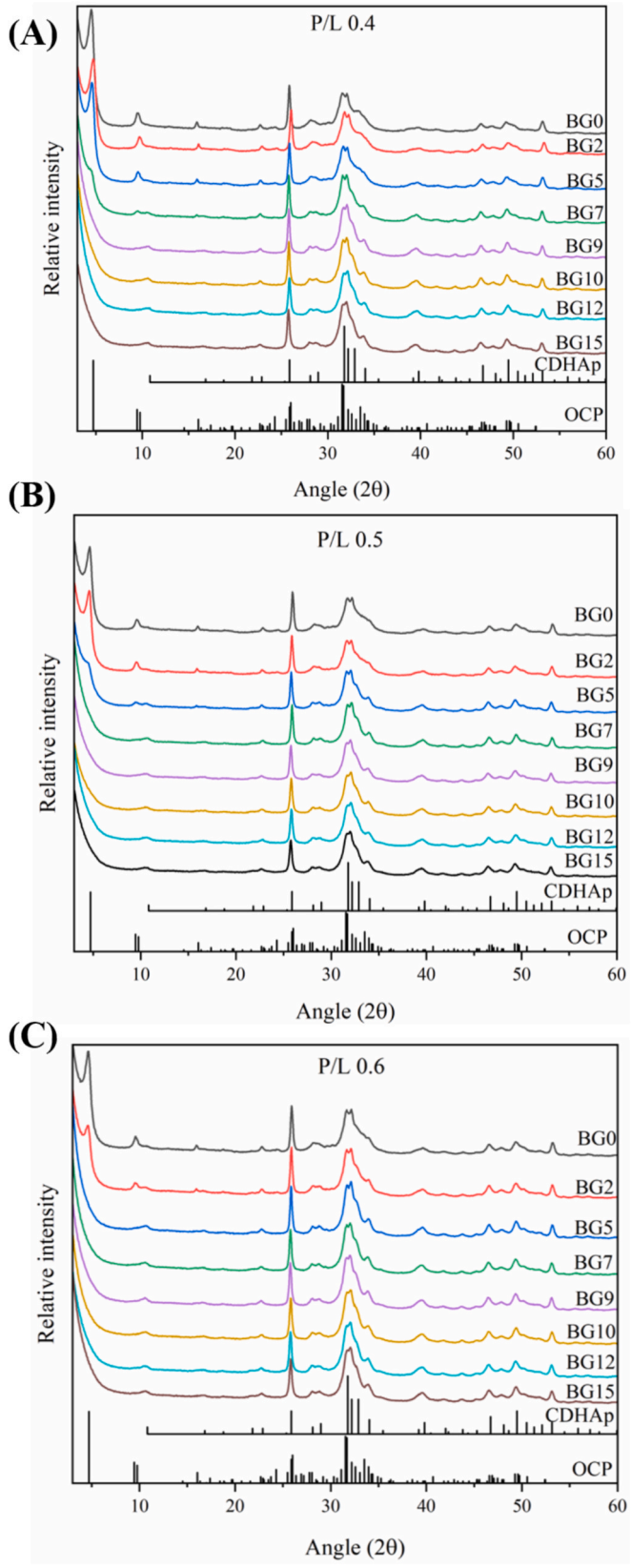

Fig. 4. XRD patterns of cement composite after setting. Cement composites prepared by using (A) P/L 0.4 g/ml; (B) P/L 0.5 g/ml; (C) P/L 0.6 g/ml.

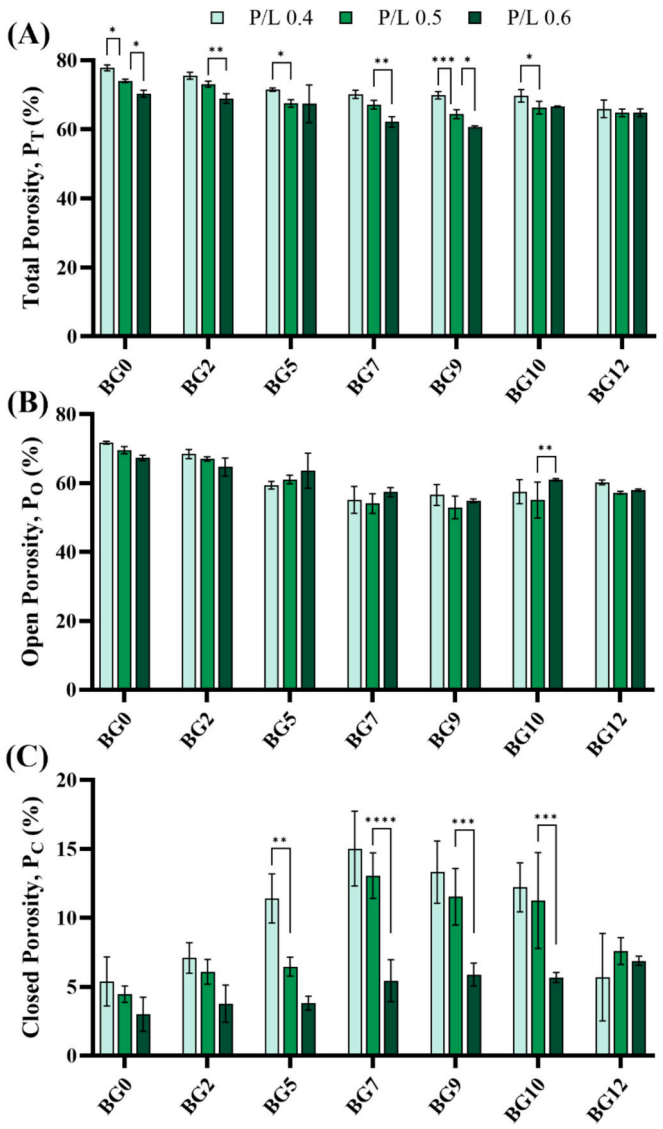

Fig. 5. Porosity (%) of the cement composites: (A) Total porosity %; (B) Open porosity % and (C) Closed porosity measurement results. n = 3, data were expressed as the mean ± SD. * represents the p-value < 0.05, ** p < 0.01, ***p < 0.001 according to the statistical analysis result of Dunnett's multiple comparison test. P_T, P_O, and P_C stand for the total porosity, open porosity and closed porosity, respectively.

trends were observed at P/L 0.5 and P/L 0.6, where BG9 achieved the lowest total porosity (64.43 ± 1.33 % at P/L 0.5; 60.73 ± 0.31 % at P/L 0.6). These findings underscore the role of 58S MBG as a structural modifier that enhances matrix densification through improved particle packing and localized ionic interactions. Partial dissolution of MBG may promote CDHAp reprecipitation within microvoids, while its fine dispersion contributes to reduced pore interconnectivity and overall porosity stabilization. Open porosity, essential for fluid exchange and bioactive ion release, varied significantly across all groups. BG0 retained the highest open porosity at all P/L ratios, with values as high as 71.74 ± 0.41 % at P/L 0.4. However, the excessive open porosity in BG0 limited its mechanical integrity, emphasizing the need for a balance between open and closed porosity. In contrast, BG9 exhibited optimal open porosity levels (52.90 ± 3.30 % at P/L 0.5), which we suggest may facilitate ion exchange while maintaining sufficient closed porosity to support enhanced compressive strength. The increased closed porosity observed in BG5, BG7 and BG9 contributed to their superior mechanical performance, reflecting a critical balance necessary for clinical

Table 3
Phase composition of cement composites after setting, expressed as the percentage of calcium deficient hydroxyapatite (CDHAp) and octacalcium phosphate (OCP) in groups containing 0–15 wt% 58S MBG (BG0–BG15) at three different powder-to-liquid (P/L) ratios (0.4, 0.5, and 0.6 g/mL). Data are presented as mean ± standard deviation.

		BG0	BG2	BG5	BG7	BG9	BG10	BG12	BG15
CDHAp Phase %	P/L 0.4	67.60 ± 3.11	72.35 ± 2.05	67.50 ± 0.71	77.28 ± 0.78	92.74 ± 1.52	92.12 ± 0.51	93.66 ± 0.30	94.22 ± 0.69
	P/L 0.5	68.40 ± 0.57	84.50 ± 7.78	79.84 ± 3.13	92.73 ± 2.23	94.66 ± 0.50	94.44 ± 0.53	94.78 ± 0.37	95.32 ± 0.25
	P/L 0.6	67.00 ± n/a	67.55 ± 1.06	93.63 ± 1.94	94.82 ± 0.73	94.92 ± 0.66	95.67 ± 0.25	94.87 ± 0.82	95.58 ± 0.16
OCP Phase %	P/L 0.4	32.40 ± 3.11	27.65 ± 2.05	32.50 ± 0.71	22.72 ± 0.78	7.27 ± 1.52	7.88 ± 0.51	6.34 ± 0.30	5.78 ± 0.69
	P/L 0.5	31.60 ± 0.57	15.50 ± 7.78	20.17 ± 3.13	7.28 ± 2.23	5.35 ± 0.50	5.57 ± 0.53	5.22 ± 0.37	4.68 ± 0.25
	P/L 0.6	33.00 ± n/a	32.45 ± 1.06	6.38 ± 1.94	5.19 ± 0.73	5.09 ± 0.66	4.33 ± 0.25	5.13 ± 0.82	4.43 ± 0.16

applications [40]. This indicates that a higher proportion of closed pores can act as stress-dissipating zones within the dense microstructure, improving load-bearing capacity and mitigating crack propagation compared to open, interconnected pores. This observation is consistent with long-term degradation studies of brushite cements performed by Ajaxon et al. [41], where a higher proportion of closed porosity was associated with slower degradation and more sustained mechanical stability over time.

The observed evolution of porosity with increasing MBG content can be explained by the dual role of MBG within the composite system. At low to moderate MBG contents (≤9 wt%), the fine MBG particles may occupy interstitial spaces between α-TCP grains, improving particle packing and thereby reducing total porosity while increasing the fraction of closed pores. This densification effect, also observed in CPC-BG systems [15,16], enhances structural integrity by decreasing pore interconnectivity. In contrast, at higher MBG contents (≥10 wt%), the trend reverses. The inherently high surface area and mesoporosity of MBG particles increase liquid retention during mixing and slow down α-TCP hydration, resulting in heterogeneous microstructures and incomplete densification of the matrix. These conditions generate micro-defects, leading to higher total porosity and compromised compressive strength, as also described in earlier studies on MBG-loaded cements [19,22]. Moreover, the strong ion-exchange capacity of mesoporous MBG, while beneficial for bioactivity, can further disrupt the uniform progression of the setting reaction at elevated concentrations [31,42]. These findings highlight that MBG plays a concentration-dependent

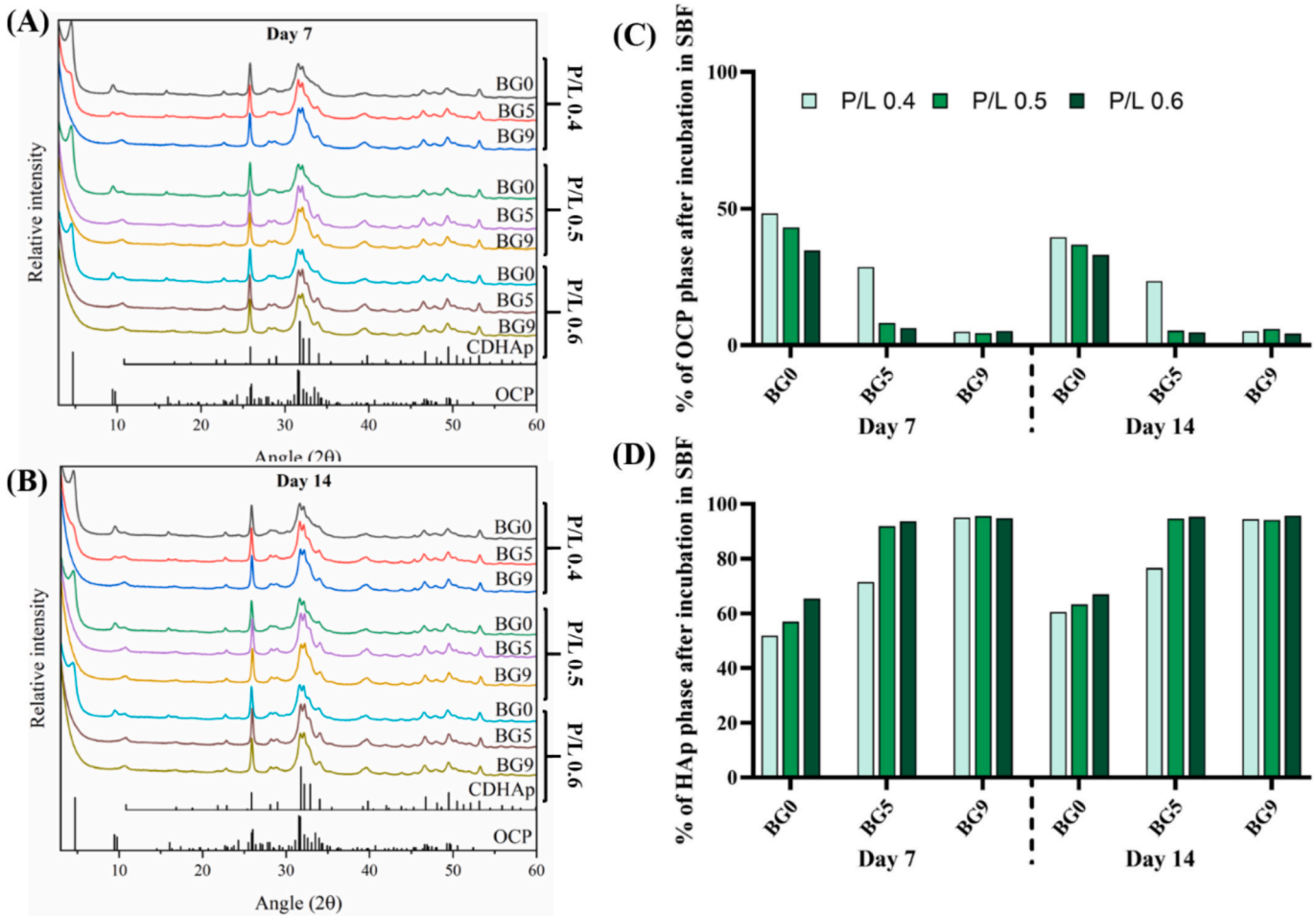

Fig. 6. XRD patterns and phase changes of cement composites: A) XRD pattern after 7 days of incubation in SBF at 37 °C; (B) XRD pattern after 14 days of incubation in SBF at 37 °C. Phase composition percentages, analyzed using Profex software [27], showing the changes in OCP and HAp phases after (C) 7 days and (D) 14 days of incubation in SBF at 37 °C.

role: acting as a densifying filler at lower contents but as a source of structural heterogeneity when present in excess.

The influence of porosity on the bioactivity and phase transformation of CPC composites was further assessed by immersing the samples in SBF (results are shown in Fig. 6). The selection of experimental groups for further analysis was guided by a comprehensive evaluation of setting time, mechanical properties, phase transformation, and microstructural characteristics. Groups with ≥ 10 wt% 58S MBG were excluded due to their excessive total porosity, disrupted phase composition, and compromised mechanical performance, making them unsuitable for further analysis. BG0, BG5, and BG9 at all P/L ratios (0.4, 0.5, and 0.6 g/mL) were initially included based on their distinct advantages observed in the earlier studies. BG0 was selected due to its high initial OCP content, which is advantageous for early-stage bioactivity despite its limitations in structural stability. BG5 and BG9 were chosen for their balanced phase composition, demonstrating a favorable ratio of OCP to CDHAp, enhanced mechanical properties, and optimal porosity levels. Obtained results revealed that, these groups exhibited consistent transformation from OCP to CDHAp, with CDHAp becoming the dominant phase after 14 days of sample immersion in SBF. The gradual phase transformation was facilitated by the optimal balance of open porosity, allowing effective ion exchange and mineral deposition. This process may also represent the natural bone remodeling mechanism, offering a scaffold that dynamically adapts to the evolving biological environment. Such adaptability positions these composites as promising candidates for applications in delayed or impaired healing scenarios, where both immediate bioactivity and long-term structural stability are essential. In contrast, BG0, characterized by high open porosity and low closed porosity, showed slower phase transformation, limiting its mineralization potential. The microstructural analysis (Fig. 7) further supports these findings. SEM images of cross-sections revealed dense and uniform microstructures in BG5 and BG9 after setting and following 14 days in SBF. Significant mineral deposition was observed in the groups containing 58S MBG (Fig. 7), indicating robust bioactivity.

Based on these findings, the selection of experimental groups for subsequent *in vitro* cell studies was guided by the presence of an initial OCP phase formation and its subsequent transformation into CDHAp. BG5 and BG9 at P/L ratios of 0.5 and 0.6 were prioritized as they demonstrated a favorable phase composition, balancing the short-term benefits of OCP with the long-term stability provided by CDHAp. These groups align with the dual-phase strategy required for clinical applications: early-stage bioactivity facilitated by OCP conversion and long-term stability ensured by the CDHAp phase. The higher CDHAp content observed in BG9 (Fig. 4) and the corresponding trend of stronger osteogenic gene expression (Fig. 9) likely stem from its more pronounced ionic exchange and surface re-mineralization behavior. Although ion-release testing was not performed for the present composites containing MBG < 20 μm, our previous study on α-TCP/MBG systems [14] with same formulation showed that the 9 wt% MBG group released up to ~ 70–75 μg/mL Ca^{2+}, ~650–700 μg/mL P^{5+}, and ~120 μg/mL Si^{4+} after 21 days. These released ions are known to enhance CDHAp precipitation and stimulate osteogenic signaling pathways such as RUNX2 and COL1 expression. Therefore, the enhanced bioactivity and phase transformation of BG9 are consistent with the previously observed ion-release behavior, although direct correlation in this study remains to be confirmed. BG0, with its high initial OCP content, highlights the potential for promoting bioactivity in early-stage bone regeneration. Although CDHAp formation was observed, its relatively lower extent in this group coincided with reduced structural performance, suggesting limited potential for long-term applications compared to BG5 and BG9.

3.3. Direct cytocompatibility of cement composites

3.3.1. 58S MBG-added cement composites enhance long-term cytocompatibility and osteogenic potential

The direct cytocompatibility of selected cement composites (BG0, BG5, and BG9) was evaluated using hMSCs from three different donors.

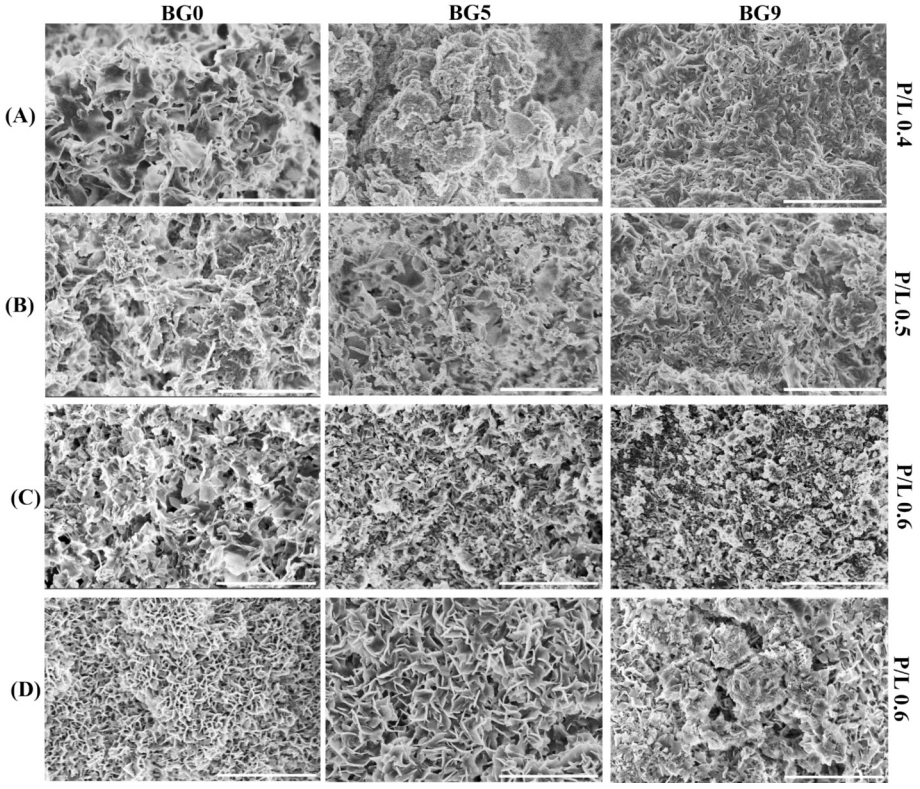

Fig. 7. Microstructure of the cross-section of bone cement composites: (A); (B) and (C) bone cement composites after setting; (D) bone cement composites after 14 days of incubation at 37°C in simulated body fluid (SBF). Scale bar: 2 μm.

Cell attachment, viability, and metabolic activity were assessed over time to investigate the interactions between the cells and the composite surfaces, with a particular focus on the influence of 58S MBG. Representative images of live (green) and dead (red) cell staining on the cement composites are shown in Fig. 8(A). On day 1, BG0 demonstrated slightly better initial cell attachment compared to BG5 and BG9, with a higher density of live cells observed. However, as the incubation period progressed to day 3, BG5 and BG9 supported a denser and more confluent layer of viable cells, while BG0 exhibited a slight decline in cell density. These trends indicate that while BG0 provides a favorable initial environment for cell attachment, 58S MBG-containing composites (BG5 and BG9) offer enhanced long-term support for cell proliferation and viability. The bioactivity of 58S MBG in BG5 and BG9 likely contributes to their long-term performance, as 58S MBG releases bioactive ions such as silicon and calcium, which stimulate cellular signaling pathways critical for proliferation and differentiation [42,43]. BG0, without 58S MBG, relies primarily on its baseline porosity and surface properties, which may limit its ability to sustain cellular activity over time. Metabolic activity, quantified using the CellTiter-Blue® assay, is presented in Fig. 8(B). At day 1, BG0 composites exhibited the highest metabolic activity compared to BG5 and BG9 across all tested powder-to-liquid (P/L) ratios. For example, at P/L 0.5, BG0 recorded a metabolic activity of 27.69 ± 2.72 a.u., outperforming BG5 (16.76 ± 1.06 a.u.) and BG9 (19.12 ± 4.28 a.u.). Similarly, at P/L 0.6, BG0 showed higher activity (21.68 ± 3.45 a.u.) compared to BG5 (19.47 ± 4.33 a.u.) and BG9 (20.42 ± 2.11 a.u.). By day 3, however, the trend shifted. BG5 and BG9 demonstrated significant increases in metabolic activity, with BG9 at P/L 0.6 reaching 42.99 ± 7.48 a.u., surpassing BG0 (38.72 ± 8.82 a.u.). The observed shift in cellular behavior, where P/L 0.6 samples of BG5 and BG9 showed higher intensity and metabolic activity than their P/L 0.5 replicates, may be attributed to the improved structural and ionic environment provided by MBG at higher cement densities. The P/L 0.6 condition likely supports a more favorable balance between bioactive ion release and scaffold architecture, enhancing long-term cellular performance. In contrast, BG0 lacks ion-releasing capacity, and its denser matrix at P/L 0.6 may have limited nutrient diffusion, slightly reducing metabolic activity. This shift suggests that while BG0 supports early metabolic activity, MBG-containing composites, particularly BG5 and BG9, provide sustained metabolic support over longer periods. The bioactive properties of 58S MBG likely play a key role in enhancing cellular performance by further releasing bioactive ions that promote cell proliferation and matrix mineralization. These findings align with prior studies that reported enhanced cell viability and proliferation on MBG-modified scaffolds. Zhang et al. [44] demonstrated that MBG incorporation improves cellular metabolic activity and osteogenic differentiation by creating a bioactive surface that closely mimics the bone mineral phase. BG0's higher initial metabolic activity may reflect its compatibility with short-term cell attachment, but the long-term advantages of MBG-containing composites make BG5 and BG9 better suited for applications requiring prolonged cellular interactions.

To further evaluate the composites' osteogenic potential, live/dead staining was performed after 7 days of culture in an osteogenic medium (Fig. 8(C)). The selection of a P/L ratio of 0.6 for this experiment was based on previous results demonstrating optimal compressive strength, porosity, and bioactivity at this ratio. Lower P/L ratios (e.g., 0.4) were excluded due to insufficient mechanical stability, while higher P/L ratios (e.g., 0.5) showed comparatively lower performance in supporting metabolic activity. P/L 0.6 provides a balance between structural integrity and biological functionality, making it ideal for studying osteogenesis. While all groups supported live cells with visible adhesion and proliferation, BG5 and BG9 exhibited significantly enhanced cell density and spreading compared to BG0. The osteoconductive advantage of MBG-containing composites becomes apparent in this context, as BG5 and BG9 provided a more supportive microenvironment for hMSCs differentiation. The release of bioactive ions from MBG is known to stimulate cellular signaling pathways, such as Wnt/β-catenin, and

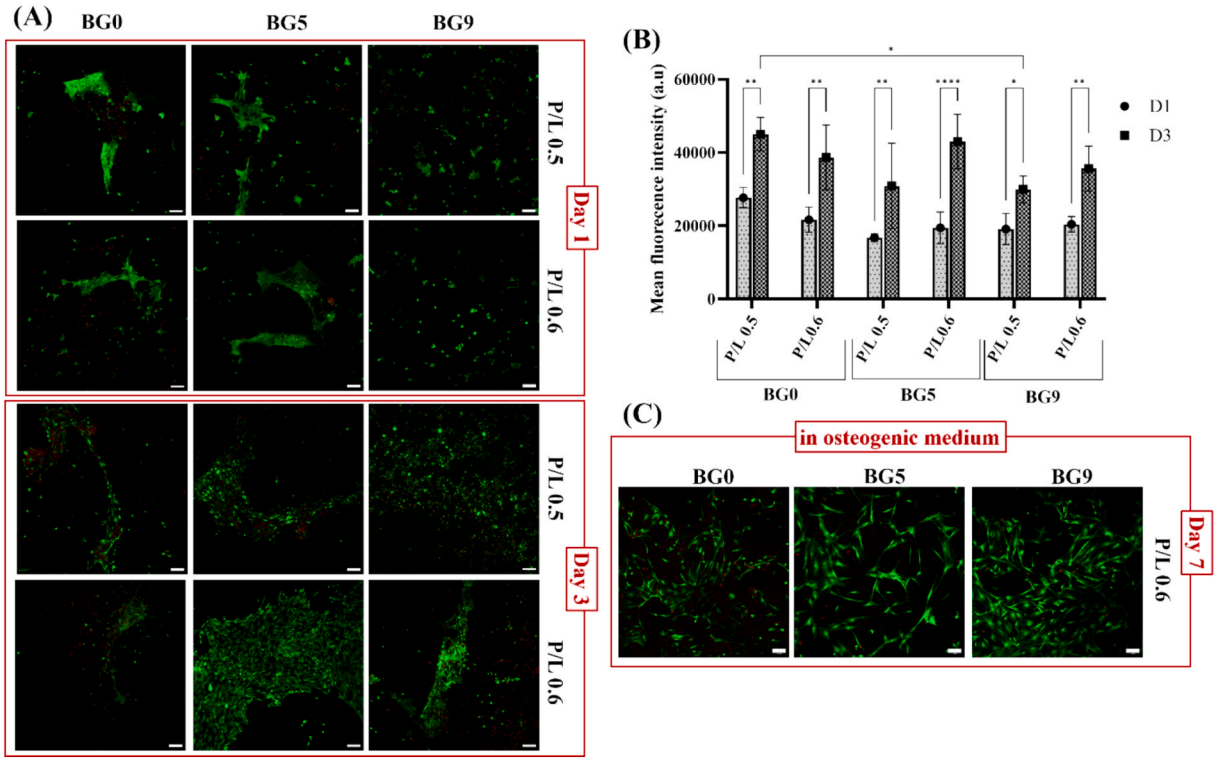

Fig. 8. Cell attachment and viability tests: (A) Representative images of live (green) and dead (red) cell staining on the cement composites on day 1 and day 3. Scale bar: 100 μm; (B) Metabolic activity of hMSCs on cement composites at day 1 and day 3 of incubation, measured using CellTiter-Blue®; (C) Representative images of live (green) and dead (red) cell staining on the cement composites prepared using P/L 0.6 g/ml on day 7. These composites were cultured in osteogenic cell culture medium. Scale bar: 100 μm. (For interpretation of the references to colour in this figure legend, the reader is referred to the web version of this article.)

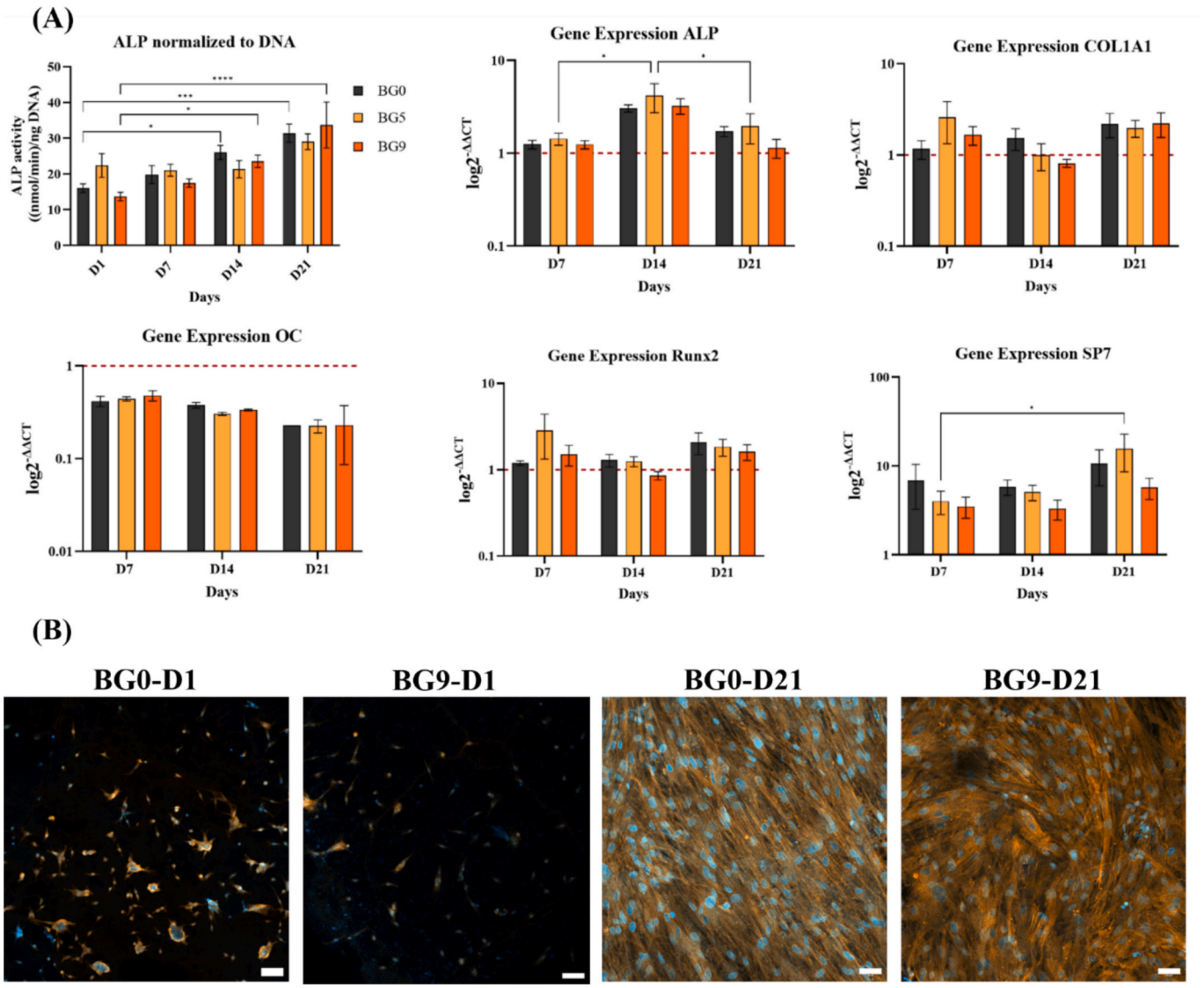

Fig. 9. Osteogenic differentiation of hMSCs on cement composites: (A) ALP activity normalized to DNA content after 7, 14, and 21 days, and gene expression of ALP, ColI, OC, Runx2, and SP7 after 7, 14, and 21 days; (B) Representative images of integrin-binding sialoprotein (IBSP) staining (orange) and nuclei counterstaining (blue) after 1 and 21 days on cement composites. Scale bar: 100 μm. (For interpretation of the references to colour in this figure legend, the reader is referred to the web version of this article.)

upregulate osteogenic markers, including ALP, Runx2, and osteocalcin [45]. These ions also contribute to the formation of a hydroxyapatite-like layer on the cement surface, further promoting osteointegration. The results of this study are consistent with previous findings [8]. For example, Yu et al. [17] demonstrated enhanced proliferation and osteogenic differentiation of osteoblasts on bioglass-containing composites. Therefore, it can be concluded that BG0 provides a strong baseline for comparison while the long-term advantages of MBG-containing composites align with the broader literature emphasizing MBG's role in enhancing bioactivity and osteogenic potential.

3.3.2. Osteogenic differentiation of hMSCs facilitated by 58S MBG modified cement composites

The osteogenic differentiation of human mesenchymal stem cells (hMSCs) cultured on selected cement composites (BG0, BG5, and BG9) with a P/L ratio of 0.6 was assessed through ALP activity, gene expression analysis, and IBSP staining. ALP activity, a key marker of early osteogenic differentiation, showed nuanced trends across the experimental groups (Fig. 9(A)). On day 1, BG0 demonstrated higher ALP activity compared to BG5 and BG9. This suggests that the inherent properties of BG0, such as higher open porosity and the absence of MBG, provided favorable conditions for an early osteogenic response. By day 7, ALP activity differences among the groups diminished, with all three groups showing comparable activity levels. This convergence indicates that while BG0 initiates differentiation effectively, MBG-modified composites (BG5 and BG9) did not show statistically significant differences in ALP activity over time under the current experimental conditions, although the visual trend suggested a slight increase in BG9 at later stages. On day 21, ALP activity appeared higher in BG9, followed by BG5, while BG0 remained relatively stable. However, the effect of 58S MBG on ALP activity remains inconclusive, as the differences were not statistically significant. ALP increased with time across all groups, indicating progression of osteogenic differentiation as the main effect. Although BG9 displayed a trend toward higher ALP at day 21, pairwise differences were not statistically significant; therefore, no clear causal relationship can be concluded. The trend is, however, consistent with BG9's combination of moderate open porosity and higher compressive strength (Figs. 5C and 3B), which likely provides both good nutrient exchange and a firm surface that encourages bone-related cell differentiation.

The gene expression of ALP provided additional insight into osteogenic differentiation, complementing the trends observed in enzymatic activity. The alignment between ALP gene expression and enzymatic activity varied slightly across time points, highlighting the complex regulation of osteogenesis where gene expression may not always directly correspond to immediate protein function. On day 7, ALP gene expression was comparable across all groups, with BG5 showing a slight increase relative to BG0 and BG9, though not markedly upregulated. Although the differences were not statistically significant, a trend of enhanced ALP gene expression in BG5 during mid-stage differentiation (day 14) was observed, suggesting a possible transcriptional influence of MBG, which warrants further validation. It is important to note that with discrete time-point analysis, transient fluctuations in gene expression or enzyme activity may have been missed. Continuous or more frequent sampling could better capture the dynamic nature of osteogenic differentiation.

The gene expression profiles of other osteogenic markers provided further context. COL1, essential for collagen synthesis and extracellular matrix formation, was consistently higher in BG9 compared to BG0 and BG5, particularly on day 7. This suggests that BG9 promotes matrix production more effectively, likely due to the bioactive properties of 58S MBG. RUNX2 expression, a transcription factor critical for early osteogenic differentiation, peaked in BG5 on day 7, aligning with its robust ALP activity and early osteogenic potential. By day 21, BG9 exhibited the highest RUNX2 expression, indicating its ability to sustain differentiation processes over time. SP7, another osteoblast-specific transcription factor, was most prominently expressed in BG5 on day 7, with BG9 maintaining moderate levels on day 21. These findings suggest that while BG5 facilitates an earlier osteogenic response, BG9 supports sustained differentiation at later stages. Notably, OC, a late-stage marker of osteogenic differentiation, remained under expressed across all groups and time points, with levels below 1. Given the low expression levels of OC across all groups and time points, it is likely that the 21-day culture period was not sufficient to capture the onset of late-stage osteoblast maturation. This aligns with previous findings suggesting that longer differentiation periods are needed to observe meaningful OC upregulation [46–48].

IBSP staining further supported these findings, highlighting both mineral deposition and extracellular matrix formation (Fig. 9(B)). On day 1, BG9 exhibited slightly more intense IBSP staining than BG0, reflecting its bioactive properties and enhanced early-stage mineralization. However, BG0 also displayed robust IBSP staining, indicating its favorable microenvironment for initiating osteogenic processes despite the absence of 58S MBG. Qualitative IBSP staining demonstrated mineralization and matrix formation in all groups by day 21. BG9 displayed marginally stronger staining than BG0; however, future image-based quantification is needed to strengthen these interpretations.

While 58S MBG addition demonstrated an effect on osteogenic differentiation, the results indicate that the impact was not significantly pronounced under the given experimental conditions. This aligns with the limited literature specifically addressing the effects of MBG on cell differentiation in calcium phosphate bone cements. However, MBG's osteoinductive potential has been widely established *in vivo* [8,15–22], demonstrating superior bone formation through bioactive ion release and the creation of a microenvironment conducive to bone regeneration. The findings of this study further support MBG's potential to enhance osteogenic differentiation *in vitro*, but they also emphasize the need for extended experimental timelines and additional studies to fully explore its osteoinductive capabilities.

In summary, while BG0 effectively initiates osteogenic differentiation, MBG-modified composites (BG5 and BG9) provide sustained transcriptional and enzymatic support for prolonged differentiation processes. BG9, in particular, demonstrates consistent upregulation of key osteogenic markers, suggesting its potential for applications requiring sustained bone regeneration. These findings contribute to the growing understanding of MBG's role in bone tissue engineering and highlight the need for further research to optimize its integration into CPC formulations.

3.3.3. Proposed mechanism linking composition, microstructure, and cell response

Moderate 58S MBG contents (5–9 wt%) increased CDHAp formation (Fig. 4; Table 3) and shifted the pore architecture toward reduced total porosity with a higher fraction of closed pores (Fig. 5), yielding a denser, more continuous matrix. We propose that these changes (i) stabilize an apatite-like surface that supports integrin-mediated adhesion (consistent with IBSP staining) and early ALP onset, and (ii) provide a mechanically supportive substrate that favors osteogenic transcriptional programs (RUNX2, COL1A1, SP7). By contrast, BG0 shows higher early attachment/metabolic readouts, likely due to greater open porosity and fluid access, but lacks the sustained ionic microenvironment and surface re-mineralization needed for later transcriptional gains.

To further substantiate these relationships, an exploratory correlation analysis using group means (BG0, BG5, BG9; P/L = 0.6) was performed (Tables 4 and 5). The results revealed a strong inverse association between CDHAp % and total porosity ($r \approx -0.76$), confirming microstructural densification with increasing MBG content. In contrast, correlations between these physicochemical parameters and osteogenic markers were weak or inconsistent ($r = -0.36$ to $+ 0.28$ for ALP and COL1A1), while RUNX2 showed a negative trend ($r \approx -0.9$). These findings indicate that, although 58S MBG addition significantly improved the structural and compositional features of the cement, these physicochemical gains did not proportionally enhance early osteogenic transcriptional activity under the tested *in vitro* conditions.

The convergence of ALP across groups by days 7–21, without robust between-group significance, suggests that once a threshold of Ca/Si/P availability and apatite coverage is reached under these *in vitro* conditions, additional MBG confers diminishing biological returns despite clear physicochemical improvements.

This *in vitro* study, limited to 21 days and lacking real-time ion-release or pH monitoring, may have missed transient pathway effects. Donor variability among hMSCs could also widen data variation; hence, non-significant trends are interpreted cautiously. Future studies combining ion-release kinetics, local pH, and focal-adhesion signaling analyses, as well as *in vivo* validation, will be essential to confirm the proposed mechanism.

4. Conclusion

This study systematically investigated the influence of 58S MBG content on the physicochemical and biological performance of α-TCP-based CPCs. CPC modification with 58S MBG significantly altered the physicochemical properties of final composite, including setting time, porosity and phase composition, with notable improvements observed in groups containing 5 wt% and 9 wt% 58S MBG (BG5 and BG9). The setting time increased proportionally with 58S MBG content, with BG9 at a powder-to-liquid ratio of 0.6 exhibiting prolonged final setting times compared to the BG0 control. Similarly, total porosity decreased with increasing MBG concentration, where BG9 reached a total porosity of approximately 60.7 %, significantly lower than BG0 at 70.3 %. Compressive strength was also enhanced in BG5 and BG9, exceeding the values measured for BG0 across all tested powder-to-liquid ratios. However, despite these physicochemical improvements, the biological findings indicated that MBG addition did not induce a significantly pronounced effect on cellular responses. This highlights the need for extended *in vitro* differentiation periods or more complex biological models are needed, as the osteoinductive potential of MBG is better documented in *in vivo* studies, where superior bone formation has been observed due to MBG's bioactive ion release capacity and surface interactions. Therefore, further research involving extended differentiation timelines and *in vivo* assessments is necessary to fully explore the potential of MBG-modified CPCs for clinical bone regeneration

Table 4
Mean ± SD of physicochemical and biological parameters used for exploratory trend analysis (P/L = 0.6).

Group	CDHAp (%) ± SD	Total Porosity (%) ± SD	ALP (Day 21, (nmol/min)/ng DNA) ± SD	ALP gene (Day 21, $\log2^{-\Delta\Delta CT}$) ± SD	RUNX2 gene (Day 21, $\log2^{-\Delta\Delta CT}$) ± SD	COL1A1 Gene (Day 21, $\log2^{-\Delta\Delta CT}$) ± SD
BG0	67 ± n/a	70.35 ± 1.04	31.39 ± 10.73	1.72 ± 0.38	2.20 ± 1.74	2.20 ± 1.74
BG5	93.63 ± 1.94	67.39 ± 5.46	40.14 ± 25.08	1.96 ± 1.22	1.98 ± 1.24	1.98 ± 1.24
BG9	94.92 ± 0.66	60.73 ± 0.31	33.67 ± 27.22	1.15 ± 0.46	2.23 ± 1.89	2.23 ± 1.89

Table 5
Exploratory correlation (r) between physicochemical and biological parameters (P/L = 0.6).

Parameter 1	Parameter 2	*r (Pearson)	Trend Interpretation
CDHAp (%)	Total Porosity (%)	–0.76	Strong negative; greater apatite = denser matrix
CDHAp (%)	ALP Activity (D21)	+0.14	Weak positive
CDHAp (%)	ALP Gene (D21)	–0.36	Weak negative
CDHAp (%)	COL1A1 Gene (D21)	+0.24	Weak positive
CDHAp (%)	RUNX2 Gene (D21)	–0.88	Strong negative
Total Porosity (%)	ALP Activity (D21)	–0.14	Weak negative
Total Porosity (%)	ALP Gene (D21)	+0.28	Weak positive
Total Porosity (%)	COL1A1 Gene (D21)	–0.15	Weak negative
Total Porosity (%)	RUNX2 Gene (D21)	+0.75	Strong positive

*r values were calculated from group mean values (BG0, BG5, BG9) to visualize linear trends between physicochemical and biological parameters.

applications.

CRediT authorship contribution statement

Öznur Demir: Writing – review & editing, Writing – original draft, Visualization, Methodology, Formal analysis, Data curation, Conceptualization. **Shahrbanoo Jahangir:** Methodology, Formal analysis. **Ezgi Irem Bektas:** Methodology, Formal analysis, Writing – review & editing. **Mauro Alini:** Writing – review & editing, Supervision. **Aldo R. Boccaccini:** Writing – review & editing, Supervision. **Dagnija Loca:** Writing – review & editing, Supervision, Resources, Conceptualization.

Declaration of competing interest

The authors declare that they have no known competing financial interests or personal relationships that could have appeared to influence the work reported in this paper.

Acknowledgements

The authors acknowledge the financial support for Open Access, the access to the infrastructure and expertise of the BBCE, stands for Baltic Biomaterials Centre of Excellence, (H2020 research and innovation programme under grant agreement No. 857287) and the Ministry of Economics of the Republic of Latvia “State research project in the field of biomedicine, medical technologies and pharmacy (BioMedPharm)” No. VPP-EM-BIOMEDICĪNA-2022/1-0001.

Data availability

Data will be made available on request.

References

[1] M. Rupp, L. Klute, S. Baertl, N. Walter, G.-K. Mannala, L. Frank, C. Pfeifer, V. Alt, M. Kerschbaum, The clinical use of bone graft substitutes in orthopedic surgery in Germany—A 10-years survey from 2008 to 2018 of 1,090,167 surgical interventions, J. Biomed. Mater. Res. Part B Appl. Biomater. 110 (2022) 350–357. https://doi.org/10.1002/jbm.b.34911.
[2] M.P. Ferraz, Bone Grafts in Dental Medicine: An Overview of Autografts, Allografts and Synthetic Materials., Mater. (Basel, Switzerland). 16 (2023). https://doi.org/10.3390/ma16114117.
[3] B.r. r,, Limitations of autograft and allograft: new synthetic solutions, Orthopedics 25 (2002) S561–S570, https://doi.org/10.3928/0147-7447-20020502-04.
[4] T. Kurien, R.G. Pearson, B.E. Scammell, Bone graft substitutes currently available in orthopaedic practice, Bone Joint J. 95-B (2013) 583–597. https://doi.org/10.1302/0301-620X.95B5.30286.
[5] R. Zhao, R. Yang, P.R. Cooper, Z. Khurshid, A. Shavandi, J. Ratnayake, Bone grafts and substitutes in dentistry: a review of current trends and developments, Molecules 26 (2021), https://doi.org/10.3390/molecules26103007.
[6] J. Zhang, W. Liu, V. Schnitzler, F. Tancret, J.M. Bouler, Calcium phosphate cements for bone substitution: chemistry, handling and mechanical properties, Acta Biomater. 10 (2014) 1035–1049, https://doi.org/10.1016/j.actbio.2013.11.001.
[7] D.-X. Lun, S.-Y. Li, N.-N. Li, L.-M. Mou, H.-Q. Li, W.-P. Zhu, H.-F. Li, Y.-C. Hu, Limitations and modifications in the clinical application of calcium sulfate, Front. Surg. 11 (2024) 1278421, https://doi.org/10.3389/fsurg.2024.1278421.
[8] Ö. Demir-Oğuz, A.R. Boccaccini, D. Loca, Injectable bone cements: what benefits the combination of calcium phosphates and bioactive glasses could bring? Bioact. Mater. 19 (2023) 217–236. https://doi.org/10.1016/j.bioactmat.2022.04.007.
[9] I. Lodoso-Torrecilla, J.J.J.P. van den Beucken, J.A. Jansen, Calcium phosphate cements: Optimization toward biodegradability, Acta Biomater. 119 (2021) 1–12, https://doi.org/10.1016/j.actbio.2020.10.013.
[10] A.B.G. de Carvalho, M. Rahimnejad, R.L.M.S. Oliveira, P. Sikder, G.S.F. A. Saavedra, S.B. Bhaduri, D. Gawlitta, J. Malda, D. Kaigler, E.S. Trichês, M. C. Bottino, Personalized bioceramic grafts for craniomaxillofacial bone regeneration, Int. J. Oral Sci. 16 (2024) 62, https://doi.org/10.1038/s41368-024-00327-7.
[11] R.F. Richter, T. Ahlfeld, M. Gelinsky, A. Lode, Composites consisting of calcium phosphate cements and mesoporous bioactive glasses as a 3D plottable drug delivery system, Acta Biomater. 156 (2023) 146–157. https://doi.org/10.1016/j.actbio.2022.01.034.
[12] F. Pupilli, A. Ruffini, M. Dapporto, M. Tavoni, A. Tampieri, S. Sprio, Design strategies and biomimetic approaches for calcium phosphate scaffolds in bone tissue regeneration, Biomimetics 7 (2022), https://doi.org/10.3390/biomimetics7030112.
[13] S. Ray, U. Thormann, I. Kramer, U. Sommer, M. Budak, M. Schumacher, A. Bernhardt, A. Lode, C. Kern, M. Rohnke, C. Heiss, K.S. Lips, M. Gelinsky, V. Alt, Mesoporous bioactive glass-incorporated injectable strontium-containing calcium phosphate cement enhanced osteoconductivity in a critical-sized metaphyseal defect in osteoporotic rats, Bioengineering 10 (2023), https://doi.org/10.3390/bioengineering10101203.
[14] Ö. Demir, E. Oselska, M. Bertins, A. Viksna, A.R. Boccaccini, D. Loca, Optimizing α-tricalcium phosphate bone cement composite formulations: the critical role of bioactive glass particle size, Mater. Des. 248 (2024) 113463, https://doi.org/10.1016/j.matdes.2024.113463.
[15] A.C.M. Renno, M.R. Nejadnik, F.C.J. Van De Watering, M.C. Crovace, E.D. Zanotto, J.P.M. Hoefnagels, J.G.C. Wolke, J.A. Jansen, J.J.J.P. Van Den Beucken, Incorporation of bioactive glass in calcium phosphate cement: Material characterization and in vitro degradation, J. Biomed. Mater. Res. - Part A. 101 A (2013) 2365–2373. https://doi.org/10.1002/jbm.a.34531.
[16] A. Sadiasa, S.K. Sarkar, R.A. Franco, Y.K. Min, B.T. Lee, Bioactive glass incorporation in calcium phosphate cement-based injectable bone substitute for improved in vitro biocompatibility and in vivo bone regeneration, J. Biomater. Appl. 28 (2014) 739–756, https://doi.org/10.1177/0885328213478256.
[17] L. Yu, Y. Li, K. Zhao, Y. Tang, Z. Cheng, J. Chen, Y. Zang, J. Wu, L. Kong, S. Liu, W. Lei, Z. Wu, A Novel injectable calcium phosphate cement-bioactive glass composite for bone regeneration, PLoS One 8 (2013), https://doi.org/10.1371/journal.pone.0062570.
[18] E.S. Sanzana, M. Navarro, F. Macule, S. Suso, J.A. Planell, M.P. Ginebra, Of the in vivo behavior of calcium phosphate cements and glasses as bone substitutes, Acta Biomater. 4 (2008) 1924–1933, https://doi.org/10.1016/j.actbio.2008.04.023.
[19] A. El-Fiqi, J.H. Kim, R.A. Perez, H.W. Kim, Novel bioactive nanocomposite cement formulations with potential properties: incorporation of the nanoparticle form of mesoporous bioactive glass into calcium phosphate cements, J. Mater. Chem. B 3 (2015) 1321–1334, https://doi.org/10.1039/c4tb01634c.

[20] M. Schumacher, L. Reither, J. Thomas, M. Kampschulte, U. Gbureck, A. Lode, M. Gelinsky, Calcium phosphate bone cement/mesoporous bioactive glass composites for controlled growth factor delivery, Biomater. Sci. 5 (2017) 578–588, https://doi.org/10.1039/C6BM00903D.
[21] T. Zhu, H. Ren, A. Li, B. Liu, C. Cui, Y. Dong, Y. Tian, D. Qiu, Novel bioactive glass based injectable bone cement with improved osteoinductivity and its in vivo evaluation, Sci. Rep. 7 (2017) 1–10, https://doi.org/10.1038/s41598-017-03207-9.
[22] R.F. Richter, C. Vater, M. Korn, T. Ahlfeld, M. Rauner, W. Pradel, B. Stadlinger, M. Gelinsky, A. Lode, P. Korn, Treatment of critical bone defects using calcium phosphate cement and mesoporous bioactive glass providing spatiotemporal drug delivery, Bioact. Mater. 28 (2023) 402–419. https://doi.org/10.1016/j.bioactmat.2023.06.001.
[23] M. Karadjian, C. Essers, S. Tsitlakidis, B. Reible, A. Moghaddam, A.R. Boccaccini, F. Westhauser, Biological properties of calcium phosphate bioactive glass composite bone substitutes: current experimental evidence, Int. J. Mol. Sci. 20 (2019) 1–22, https://doi.org/10.3390/ijms20020305.
[24] Ö. Demir, A. Pylostomou, D. Loca, Octacalcium phosphate phase forming cements as an injectable bone substitute materials: preparation and in vitro structural study, Biomater. Adv. 157 (2024), https://doi.org/10.1016/j.bioadv.2023.213731.
[25] J. Locs, V. Zalite, L. Berzina-Cimdina, M. Sokolova, Ammonium hydrogen carbonate provided viscous slurry foaming-a novel technology for the preparation of porous ceramics, J. Eur. Ceram. Soc. 33 (2013) 3437–3443, https://doi.org/10.1016/j.jeurceramsoc.2013.06.010.
[26] T. Kokubo, H. Takadama, How useful is SBF in predicting in vivo bone bioactivity? Biomaterials 27 (2006) 2907–2915, https://doi.org/10.1016/j.biomaterials.2006.01.017.
[27] N. Doebelin, R. Kleeberg, Profex: a graphical user interface for the Rietveld refinement program BGMN, J. Appl. Crystallogr. 48 (2015) 1573–1580, https://doi.org/10.1107/S1600576715014685.
[28] W. Xia, J. Chang, Preparation, in vitro bioactivity and drug release property of well-ordered mesoporous 58S bioactive glass, J. Non Cryst. Solids 354 (2008) 1338–1341. https://doi.org/10.1016/j.jnoncrysol.2006.10.084.
[29] Q. Wa, Y. Luo, Y. Tang, J. Song, P. Zhang, X. Linghu, S. Lin, G. Li, Y. Wang, Z. Wen, S. Huang, W. Xu, Mesoporous bioactive glass-enhanced MSC-derived exosomes promote bone regeneration and immunomodulation in vitro and in vivo, J. Orthop. Transl. 49 (2024) 264–282. https://doi.org/10.1016/j.jot.2024.09.009.
[30] M. Bohner, F. Bigolin, I. Bohner, T. Imwinkelried, Y. Maazouz, P. Michel, C. Stähli, Y. Viecelli, N. Döbelin, The reactivity of α-tricalcium phosphate powders is affected by minute amounts of β-calcium pyrophosphate and by the synthesis temperature, Open Ceram. 19 (2024) 100647. https://doi.org/10.1016/j.oceram.2024.100647.
[31] Q.H. Shi, J.F. Wang, J.P. Zhang, J. Fan, G.D. Stucky, Rapid-setting, mesoporous, bioactive glass cements that induce accelerated in vitro apatite formation, Adv. Mater. 18 (2006) 1038–1042. https://doi.org/10.1002/adma.200502292.
[32] L.-C. Gerhardt, A.R. Boccaccini, Bioactive glass and glass-ceramic scaffolds for bone tissue engineering, Mater 3 (2010), https://doi.org/10.3390/ma3073867.
[33] C. Vater, A. Lode, A. Bernhardt, A. Reinstorf, B. Nies, M. Gelinsky, Modifications of a calcium phosphate cement with biomolecules-Influence on nanostructure, material, and biological properties, J. Biomed. Mater. Res. – Part A. 95 (2010) 912–923, https://doi.org/10.1002/jbm.a.32920.
[34] K. Tsuru, M. Ruslin, S. Maruta, K.I. Matsuya, Effects of the method of apatite seed crystals addition on setting reaction of α-tricalcium phosphate based apatite cement, J. Mater. Sci. Mater. Med. 26 (2015) 244, https://doi.org/10.1007/s10856-015-5570-8.
[35] I. Kovrlija, J. Locs, D. Loca, Octacalcium phosphate: innovative vehicle for the local biologically active substance delivery in bone regeneration, Acta Biomater. 135 (2021) 27–47. https://doi.org/10.1016/j.actbio.2021.08.021.
[36] T. Yokoi, T. Goto, T. Kato, S. Takahashi, J. Nakamura, T. Sekino, C. Ohtsuki, M. Kawashita, Hydroxyapatite formation from octacalcium phosphate and its related compounds: a discussion of the transformation mechanism, Bull. Chem. Soc. Jpn 93 (2020) 701–707, https://doi.org/10.1246/bcsj.20200031.
[37] L.C. Palmer, C.J. Newcomb, S.R. Kaltz, E.D. Spoerke, S.I. Stupp, Biomimetic systems for hydroxyapatite mineralization inspired by bone and enamel, Chem. Rev. 108 (2008) 4754–4783, https://doi.org/10.1021/cr8004422.
[38] O. Suzuki, S. Kamakura, T. Katagiri, M. Nakamura, B. Zhao, Y. Honda, R. Kamijo, Bone formation enhanced by implanted octacalcium phosphate involving conversion into Ca-deficient hydroxyapatite, Biomaterials 27 (2006) 2671–2681, https://doi.org/10.1016/j.biomaterials.2005.12.004.
[39] M.C. Tronco, J.B. Cassel, L.A. dos Santos, α-TCP-based calcium phosphate cements: a critical review, Acta Biomater. 151 (2022) 70–87. https://doi.org/10.1016/j.actbio.2022.08.040.
[40] C. Dall'Oca, T. Maluta, F. Cavani, G.P. Morbioli, P. Bernardi, A. Sbarbati, D. Degl'Innocenti, B. Magnan, The biocompatibility of porous vs non-porous bone cements: a new methodological approach, Eur. J. Histochem. 58 (2014) 2255, https://doi.org/10.4081/ejh.2014.2255.
[41] I. Ajaxon, C. Öhman, C. Persson, Long-term in vitro degradation of a high-strength brushite cement in water, PBS, and Serum SOLution, Biomed Res. Int. 2015 (2015), https://doi.org/10.1155/2015/575079.
[42] M. Vallet-Regi, A.J. Salinas, Mesoporous bioactive glasses for regenerative medicine, Mater. Today Bio 11 (2021) 100121. https://doi.org/10.1016/j.mtbio.2021.100121.
[43] E. Piatti, M. Miola, E. Verné, Tailoring of bioactive glass and glass-ceramics properties for in vitro and in vivo response optimization: a review, Biomater. Sci. 12 (2024) 4546–4589, https://doi.org/10.1039/d3bm01574b.
[44] X. Zhang, Y. Chen, J. Fu, Q. Chen, Y. Li, C. Fang, C. Li, L. Wang, D. Qiu, Z. Zhang, An injectable pH neutral bioactive glass-based bone cement with suitable bone regeneration ability, J. Orthop. Transl. 36 (2022) 120–131. https://doi.org/10.1016/j.jot.2022.05.011.
[45] P.S. Lee, C. Heinemann, K. Zheng, R. Appali, F. Alt, J. Krieghoff, A. Bernhardt, A. R. Boccaccini, U. van Rienen, V. Hintze, The interplay of collagen/bioactive glass nanoparticle coatings and electrical stimulation regimes distinctly enhanced osteogenic differentiation of human mesenchymal stem cells, Acta Biomater. 149 (2022) 373–386. https://doi.org/10.1016/j.actbio.2022.06.045.
[46] K. Kaur, S. Das, S. Ghosh, Regulation of human osteoblast-to-osteocyte differentiation by direct-write 3D microperiodic hydroxyapatite scaffolds, ACS Omega 4 (2019) 1504–1515, https://doi.org/10.1021/acsomega.8b03272.
[47] P. Zhou, J.-M. Shi, J.-E. Song, Y. Han, H.-J. Li, Y.-M. Song, F. Feng, J.-L. Wang, R. Zhang, F. Lan, Establishing a deeper understanding of the osteogenic differentiation of monolayer cultured human pluripotent stem cells using novel and detailed analyses, Stem Cell Res. Ther. 12 (2021) 41, https://doi.org/10.1186/s13287-020-02085-9.
[48] Y.-T. Tsao, Y.-J. Huang, H.-H. Wu, Y.-A. Liu, Y.-S. Liu, O.K. Lee, Osteocalcin mediates biomineralization during osteogenic maturation in human mesenchymal stromal cells, Int. J. Mol. Sci. 18 (2017), https://doi.org/10.3390/ijms18010159.